UNIVERSITY OF THESSALY

SCHOOL OF ENGINEERING

DEPARTMENT OF MECHANICAL ENGINEERING

MODELING OF STRESS-STRAIN RESPONSE AND MARTENSITIC TRANSFORMATION KINETICS IN AUSTENITIC STEELS

by

CHRISTOS DEMIRIS

Submitted in partial fulfillment of the requirements for the degree of Diploma in Mechanical Engineering at the University of Thessaly

Volos, 2025

Institutional Repository - Library & Information Centre - University of Thessaly
13/09/2026 18:03:45 EEST - 216.73.216.14

UNIVERSITY OF THESSALY

SCHOOL OF ENGINEERING

DEPARTMENT OF MECHANICAL ENGINEERING

MODELING OF STRESS-STRAIN RESPONSE AND MARTENSITIC TRANSFORMATION KINETICS IN AUSTENITIC STEELS

by

CHRISTOS DEMIRIS

Submitted in partial fulfillment of the requirements for the degree of Diploma in Mechanical Engineering at the University of Thessaly

Volos, 2025

Institutional Repository - Library & Information Centre - University of Thessaly
13/09/2026 18:03:45 EEST - 216.73.216.14

© 2025 Christos Demiris

All rights reserved. The approval of the present D Thesis by the Department of Mechanical Engineering, School of Engineering, University of Thessaly, does not imply acceptance of the views of the author (Law 5343/32 art. 202).

Institutional Repository - Library & Information Centre - University of Thessaly
13/09/2026 18:03:45 EEST - 216.73.216.14

Approved by the Committee on Final Examination:

Advisor	Dr. Gregory N. Haidemenopoulos, Professor, Department of Mechanical Engineering, University of Thessaly
Member	Dr. Nikolaos Aravas, Professor, Department of Mechanical Engineering, University of Thessaly
Member	Dr. Eleni Kamoutsi, Lab Teaching Personnel, Department of Mechanical Engineering, University of Thessaly

Date Approved: [05, 26, 2025]

Institutional Repository - Library & Information Centre - University of Thessaly
13/09/2026 18:03:45 EEST - 216.73.216.14

Acknowledgements

Firstly, I would like to express my sincere gratitude to my supervisor, **Dr. Gregory N. Haidemenopoulos**, for his invaluable guidance, continuous support, and the opportunity to undertake this thesis under his supervision. His expertise and insight have been essential throughout this journey.

I would also like to sincerely thank the members of the examination committee, **Dr. Nikolaos Aravas** and **Dr. Eleni Kamoutsi**, for their careful review of this thesis and for the valuable knowledge and guidance they offered me throughout my years of study.

I am also deeply thankful to **Dr. Sotiria Houliara** for her unwavering support, mentorship, and encouragement throughout my final year of studies.

My heartfelt appreciation goes to the friends who have stood beside me throughout this long and challenging academic path. I am especially grateful to **Eleftherios Tsompanis**, not only for introducing me to MATLAB with unmatched clarity but also for being a constant source of support from the very beginning. To **Dorothea Kleinaki**, a truly special person, I extend my warmest thanks for her patience, positivity, and encouragement during the final stretch of this journey. I also wish to thank **George Ntritsos** for the many shared hours in the laboratory, filled with both meaningful discussions and mutual concerns about the future.

To my teammates from the **HERMES student team**, I am thankful for the knowledge we built together and the goals we pursued in unity. I also acknowledge my **colleagues at work** for their understanding and for enabling me to balance professional responsibilities with academic progress.

To my **parents, Nikos and Maria**, I owe everything. Their sacrifices, love, and constant support have made this journey possible. To my **sister, Konstantina**, thank you for all the memories and moments we've shared.

Finally, I dedicate this thesis to my high school mathematics teacher, **Konstantinos Polychronou**, whose belief in me and passion for science inspired my path. His presence and encouragement made this dream a reality.

Institutional Repository - Library & Information Centre - University of Thessaly
13/09/2026 18:03:45 EEST - 216.73.216.14

MODELING OF STRESS-STRAIN RESPONSE AND MARTENSITIC TRANSFORMATION KINETICS IN AUSTENITIC STEELS

CHRISTOS DEMIRIS

Department of Mechanical Engineering, University of Thessaly

Supervisor: Dr Gregory N. Haidemenopoulos,

Professor of Metallurgy

Abstract

Cryogenic storage of liquefied fuels such as LNG, LPG, and hydrogen imposes extreme mechanical and environmental demands on structural materials. Austenitic and duplex stainless steels are widely used in such applications due to their high toughness and resistance to brittle fracture at sub-zero temperatures. However, metastable austenite may transform into martensite under stress or strain, altering the material's ductility and mechanical stability. To address this, the present study investigates the transformation behavior and mechanical response of five fully austenitic stainless steels-AISI 201, 304, 304L, 316, and 316L-as well as a custom duplex stainless steel compositionally similar to Duplex 2205.

A computational model was developed in MATLAB, incorporating thermodynamic calculations of stacking fault energy (SFE) and a constitutive model for martensitic transformation kinetics based on prior work by Aristeidakis and Haidemenopoulos. The model simulates the evolution of ε- and α′-Martensite, twinning, stress–strain behavior, and work-hardening rate as functions of strain and temperature. In the absence of experimental stress–strain data, default material parameters were used to ensure consistency across all alloys.

Simulation results reveal a strong correlation between martensite formation and mechanical performance. AISI 304L emerged as the most favorable austenitic grade, exhibiting slow transformation kinetics, delayed hardening, and high phase stability across sub-zero temperatures. When the duplex stainless steel is included, it outperforms all others due to its inherently limited austenite fraction and higher SFE, confirming its suitability for cryogenic service. These findings provide a valuable comparative framework for selecting stainless steel alloys in the design of next-generation cryogenic storage systems.

Institutional Repository - Library & Information Centre - University of Thessaly
13/09/2026 18:03:45 EEST - 216.73.216.14

ΜΟΝΤΕΛΟΠΟΙΗΣΗ ΤΗΣ ΑΠΟΚΡΙΣΗΣ ΤΑΣΗΣ-ΠΑΡΑΜΟΡΦΩΣΗΣ ΚΑΙ ΤΗΣ ΚΙΝΗΤΙΚΗΣ ΤΟΥ ΜΑΡΤΕΝΣΙΤΙΚΟΥ ΜΕΤΑΣΧΗΜΑΤΙΣΜΟΥ ΣΕ ΩΣΤΕΝΙΤΙΚΟΥΣ ΧΑΛΥΒΕΣ

ΧΡΗΣΤΟΣ ΔΕΜΙΡΗΣ

Τμήμα Μηχανολόγων Μηχανικών, Πανεπιστήμιο Θεσσαλίας, 2025

Επιβλέπων Καθηγητής: Δρ. Γρηγόρης Ν. Χαϊδεμενόπουλος,

Καθηγητής Φυσικής Μεταλλουργίας

Περίληψη

Η κρυογονική αποθήκευση υγροποιημένων καυσίμων, όπως LNG, LPG και υδρογόνου, επιβάλλει ιδιαίτερες μηχανικές και περιβαλλοντικές απαιτήσεις στα δομικά υλικά. Οι ωστενιτικοί και διφασικοί ανοξείδωτοι χάλυβες χρησιμοποιούνται ευρέως σε τέτοιες εφαρμογές, λόγω της υψηλής ανθεκτικότητας τους στην ψαθυρή θραύση σε χαμηλές θερμοκρασίες. Ωστόσο, η μετάσταση της ωστενιτικής φάσης ενδέχεται να οδηγήσει σε μετασχηματισμό σε μαρτενσίτη υπό την επίδραση τάσης ή παραμόρφωσης, μεταβάλλοντας τη δυσκαμψία και τη μηχανική σταθερότητα του υλικού. Στο πλαίσιο αυτό, η παρούσα μελέτη διερευνά τη συμπεριφορά μετασχηματισμού και τη μηχανική απόκριση πέντε πλήρως ωστενιτικών ανοξείδωτων χαλύβων -AISI 201, 304, 304L, 316 και 316L- καθώς και ενός ειδικά σχεδιασμένου διφασικού χάλυβα με σύνθεση παρόμοια με τον εμπορικό Duplex 2205.

Αναπτύχθηκε υπολογιστικό μοντέλο στο MATLAB, το οποίο ενσωματώνει θερμοδυναμικό υπολογισμό της ενέργειας ατελειών στοίβαξης (SFE) και ένα φυσικό μοντέλο κινητικής μετασχηματισμού μαρτενσίτη, βασισμένο στο έργο των Αριστειδάκη και Χαϊδεμενόπουλου. Το μοντέλο προσομοιώνει την εξέλιξη των φάσεων ε- και α′-Μαρτενσίτη, τη δημιουργία διδύμων, τις καμπύλες τάσης–παραμόρφωσης και τον ρυθμό σκλήρυνσης κατά την παραμόρφωση, ως συνάρτηση της θερμοκρασίας και της ολκής. Ελλείψει πειραματικών δεδομένων, χρησιμοποιήθηκαν προκαθορισμένες τιμές παραμέτρων για τη διατήρηση της συγκρισιμότητας μεταξύ των κραμάτων.

Τα αποτελέσματα έδειξαν σαφή συσχέτιση μεταξύ του βαθμού μετασχηματισμού μαρτενσίτη και της μηχανικής απόκρισης. Το κράμα AISI 304L εμφάνισε την πιο ευνοϊκή συμπεριφορά από τους ωστενιτικούς χάλυβες, παρουσιάζοντας αργή κινητική μετασχηματισμού, καθυστερημένο σκλήρυνση και υψηλή σταθερότητα φάσης. Όταν συμπεριλήφθηκε ο διφασικός χάλυβας, ξεπέρασε σε απόδοση τα υπόλοιπα λόγω της περιορισμένης ωστενιτικής φάσης και του υψηλότερου SFE, επιβεβαιώνοντας την καταλληλότητά του για κρυογονικές εφαρμογές. Τα συμπεράσματα της παρούσας εργασίας παρέχουν ένα πολύτιμο συγκριτικό εργαλείο για την επιλογή χαλύβων σε συστήματα αποθήκευσης καυσίμων νέας γενιάς.

Institutional Repository - Library & Information Centre - University of Thessaly
13/09/2026 18:03:45 EEST - 216.73.216.14

Institutional Repository - Library & Information Centre - University of Thessaly
13/09/2026 18:03:45 EEST - 216.73.216.14

Table of Contents

Institutional Repository - Library & Information Centre - University of Thessaly
13/09/2026 18:03:45 EEST - 216.73.216.14

LIST OF TABLES

Institutional Repository - Library & Information Centre - University of Thessaly
13/09/2026 18:03:45 EEST - 216.73.216.14

LIST OF FIGURES

Institutional Repository - Library & Information Centre - University of Thessaly
13/09/2026 18:03:45 EEST - 216.73.216.14

Chapter 1. Introduction

1.1 Problem Definition

Cryogenic storage containers for liquefied fuels represent a critical component of modern energy infrastructure. With the increasing use of liquefied hydrogen (LH_2), liquefied natural gas (LNG), and liquefied petroleum gas (LPG) as alternative and transitional fuels, there is a growing demand for materials that can safely operate under extremely low temperatures. These applications impose strict requirements on the mechanical performance of container materials, particularly in terms of ductility, fracture toughness, and resistance to phase transformations (martensitic) that may compromise structural integrity.

Therefore, it is essential to evaluate and identify suitable austenitic steel alloys that can retain favorable mechanical properties under cryogenic conditions. This necessitates a systematic investigation into candidate materials, examining their microstructural stability and deformation mechanisms-especially those associated with martensitic transformations and twinning effects during loading.

1.2 Objectives

Fig. 1: LNG Storage Tanks

The primary objective of this thesis is to identify the optimal austenitic steel alloy for the safe storage of liquefied fuels- liquid hydrogen (LH_2), liquefied natural gas (LNG), or liquefied petroleum gas (LPG)-under cryogenic conditions. The extreme thermal environment to which these storage systems are subjected necessitates the use of materials that maintain adequate ductility throughout their service life. Austenitic stainless steels are known for their favorable mechanical properties and corrosion resistance at low temperatures; however, they are also susceptible to phase transformations under mechanical loading. In particular, the formation of ε-Martensite and α′-Martensite through stress-assisted and strain-induced mechanisms, as well as twinning, can significantly compromise ductility and, consequently, structural integrity. Therefore, minimizing these transformations is critical to ensuring the mechanical reliability and long-term performance of cryogenic fuel containment systems.

To identify the most suitable austenitic steel grade for cryogenic fuel storage applications, a computational constitutive model was developed and implemented in MATLAB. The model is based on the work of John S. Aristeidakis and Gregory N. Haidemenopoulos [2] and was appropriately adapted for the objectives of this research. Specifically, the model was modified to incorporate predefined compositions for five commercially relevant austenitic stainless steel

Institutional Repository - Library & Information Centre - University of Thessaly
13/09/2026 18:03:45 EEST - 216.73.216.14

grades: AISI 201, 304, 304L, 316, and 316L. A custom Duplex stainless steel was also considered. These alloys were subjected to a series of numerical simulations over a range of temperatures, primarily sub-zero, to assess their performance under cryogenic conditions.

The simulations aimed to evaluate the transformation kinetics of martensitic phases (ε- and α′-Martensite) resulting from the transformation-induced plasticity (TRIP) and twinning-induced plasticity (TWIP) effects. Key outputs of the model include the final volume fractions of the transformed phases, the stress–strain response, and the associated work-hardening behavior. These results serve as critical indicators of the alloys' mechanical stability and ductility, which are essential for ensuring the structural integrity of cryogenic storage systems.

To determine the most appropriate austenitic steel alloy for cryogenic liquefied fuel storage applications, a comparative assessment of simulation data was performed. The key parameters analyzed include:

- **Global Volume Fraction of Strain Induced Phases**: The evolution of the ε-, α'-Martensite and twins phase fractions was examined as a function of the applied nominal strain. This evaluation helps identify the susceptibility of each alloy to martensitic transformation under mechanical loading.
- **Stress-Strain Response**: Both nominal and true stress-strain curves were analyzed to characterize the elastoplastic behavior of each alloy under cryogenic and sub-zero temperatures.
- **Work Hardening Rate (dσ/dε)**: The rate of strain hardening was evaluated with respect to the applied true strain, offering insights into the alloy's capacity to resist further plastic deformation during operation.
- **α'-Martensite Evolution at Sub-Zero Temperatures**: The progression of α'-Martensite volume fraction was monitored over a range of sub-zero temperatures, in order to evaluate the thermal sensitivity of the transformation kinetics and phase stability.

These parameters collectively support a comprehensive understanding of the mechanical and microstructural stability of the aforementioned candidate alloys.

The alloys' compositions, considered in this study, are presented below. The concentrations of the principal alloying elements (C, Mn, Al, Si, Ni, Cr, Mo, and N) are given in weight percent (%wt):

Table. 1: Austenitic Alloys Composition

Alloy	***C (%)***	***Mn (%)***	***Al (%)***	***Si (%)***	***Ni (%)***	***Cr (%)***	***Mo (%)***	***N (%)***
AISI 201	0.0237	7.018	0.0047	0.382	4.07	17.06	0.0429	0.164
304	0.08	2	0.04	0.75	8	18	-	0.1
304L	0.03	2	0.04	0.75	9	18	-	0.1
316	0.08	2	0.04	0.75	10.5	17.5	2.5	0.1
316L	0.03	2	0.04	0.75	10	16	2	0.1
Duplex SS	0.017	1.25	0.005	0.34	7.52	23.78	3.12	0.23

These concentrations form the input basis for the model used in this study.

Institutional Repository - Library & Information Centre - University of Thessaly
13/09/2026 18:03:45 EEST - 216.73.216.14

Chapter 2. Literature Review – State of the Art

2.1 Austenitic steels in cryogenic applications

Cryogenic storage of liquefied fuels such as hydrogen, natural gas, and petroleum derivatives imposes extreme mechanical and environmental demands on containment materials. Among the most important material properties required for such applications are high fracture toughness, retained ductility at low temperatures, and resistance to phase transformations that could compromise mechanical integrity.

Over the past decades, austenitic stainless steels have emerged as primary candidates for cryogenic storage due to their face-centered cubic (FCC) crystal structure, which imparts exceptional toughness even at temperatures approaching absolute zero. However, metastability of the austenite phase introduces uncertainty in mechanical behavior. Retained austenite may transform into α′-Martensite or form mechanical twins under loading, depending on the stacking fault energy (SFE), alloy composition, and temperature. This can lead to increased strength due to the TRIP and TWIP effects. However, it may reduce ductility, a key concern for pressure vessels and pipelines storing liquefied gases.

2.2 TRIP and TWIP Mechanisms in Metastable Austenitic Steels

Metastable austenitic steels are known to have two key deformation mechanisms-Transformation-Induced Plasticity (TRIP) and Twinning-Induced Plasticity (TWIP)-which affect the material's ability to achieve high strength while maintaining ductility. These mechanisms are closely linked to the stability of austenite, which is influenced by temperature, chemical composition, and stacking fault energy (SFE).

2.2.1 Transformation-Induced Plasticity (TRIP)

The TRIP effect involves the strain- or stress-induced transformation of retained austenite into martensitic phases-primarily ε-Martensite and α′-Martensite-during plastic deformation. This transformation contributes to additional strain hardening and postpones the onset of localized necking, thereby enhancing both strength and ductility. The TRIP effect is dominant in steels with low to moderate SFE, where austenite is sufficiently unstable under mechanical loading. This behavior is particularly pronounced at low or cryogenic temperatures, where the driving force for martensitic transformation increases. TRIP is a desirable mechanism in steels intended for applications requiring energy absorption and resistance to brittle fracture.

2.2.2 Twinning-Induced Plasticity (TWIP)

The TWIP effect occurs in steels with moderate to high SFE, where the martensitic transformation is suppressed. In this case, plastic deformation is accommodated through the formation of mechanical twins within the austenite matrix. These twins act as strong barriers to dislocation motion, leading to a continuous increase in work hardening. TWIP enables exceptional ductility and strength retention over a wide strain range, making it a key mechanism in high-Mn fully austenitic steels.

Institutional Repository - Library & Information Centre - University of Thessaly
13/09/2026 18:03:45 EEST - 216.73.216.14

2.2.3 Interaction Between TRIP and TWIP

In many modern austenitic steels, particularly those used in cryogenic or high-performance structural applications, TRIP and TWIP may act simultaneously or sequentially, depending on the deformation conditions and alloy design.

- At lower SFE, ε-Martensite may form initially, followed by the transformation to α′-Martensite (TRIP-dominated behavior).
- At intermediate SFE, mechanical twinning may occur first, providing initial hardening, with transformation to martensite occurring later in the strain history.

The controlled activation of these mechanisms allows for the design of steels that exhibit a favorable balance between strength, ductility, and toughness.

Table. 2: TRIP and TWIP effects in austenitic steels comparison

	TRIP Transformation-Induced Plasticity	**TWIP Twinning-Induced Plasticity**
Mechanism	Phase Transformation Austenite to α'-, ε-Martensite	Formation of deformation twins within austenite
Crystal Structure	Metastable FCC austenite	Stable FCC austenite
Driving Force	Mechanical Strain→Transformation	Mechanical Strain→ Mechanical Twinning
SFE	15-30 mJ/m^2	20-45 mJ/m^2
Microstructural Form	Martensite laths in retained austenite	Parallel or intersecting twin bands in grains

2.3 Stacking Fault Energy of Austenite

The stacking fault energy (SFE) of austenite was previously calculated by Haidemenopoulos et al. [1] in a computational framework developed specifically for the design of medium manganese (Mn) steels. This model is thermodynamically grounded and is based on the classic Olson–Cohen [3] equation, which relates the driving force for the austenite-to-ε-Martensite transformation to alloy composition, temperature, and interfacial energy considerations.

The approach accounts for contributions from chemical, magnetic, and excess energy terms, each influenced by the austenite's grain size and elemental composition. The resulting SFE prediction allows for evaluating austenite stability, which is crucial for understanding the activation of deformation mechanisms such as mechanical twinning, ε-Martensite, or α′-Martensite formation.

Institutional Repository - Library & Information Centre - University of Thessaly
13/09/2026 18:03:45 EEST - 216.73.216.14

2.4 Existing models for martensitic transformations

Accurate prediction of the phase fraction of α′-Martensite formed during deformation is critical for assessing the mechanical behavior and microstructural evolution of austenitic steels. The present study relies heavily on the foundational work of John S. Aristeidakis and Gregory N. Haidemenopoulos, who developed a physically based model to simulate the kinetics of stress-assisted and strain-induced α′-martensitic transformation.

Several attempts have been made to model the deformation behavior and transformation kinetics of steels containing austenite under uniaxial tension. Early approaches, such as the Olson-Cohen [3] model, introduced empirical formulations to capture the kinetics of strain-induced martensitic transformation. These models often required fitting to experimental data and lacked a direct link to microstructural variables. Extensions and modifications of this model, such as those implemented by Zecevic et al. [4], incorporated crystallographic information to improve predictive capabilities within a crystal plasticity framework.

In addition, constitutive models based on dislocation dynamics have been widely used. The Kocks-Mecking-Estrin model [5,6,7,8], which links dislocation density evolution to macroscopic flow behavior, has been employed to simulate the stress-strain response in steels with varying austenite stability. These models, while effective for describing general trends, typically do not resolve individual transformation pathways such as TRIP or TWIP unless supplemented by empirical or semi-empirical kinetic equations.

More physically grounded approaches have been explored to capture the complexity of phase transformations in advanced high-strength steels (AHSS). Galindo-Nava and Rivera-Díaz-del-Castillo [9] proposed a model accounting for the progressive activation and interaction of martensitic and twinning mechanisms via shear band formation. Their approach allows for simultaneous prediction of stress-strain behavior and phase fraction evolution (α′- and ε-Martensite, and twins) without relying on computationally intensive crystal plasticity.

Further advances include the work of Papadioti et al. [10] and Tzini et al. [11], who applied transformation kinetics models to multi-phase TRIP steels and austenite particle distributions obtained from multi-phase field simulations. These models linked microstructural features such as grain size, phase composition, and stacking fault energy (SFE) to mechanical behavior, capturing the role of stress-assisted and strain-induced transformations in plastic flow.

The physically based model presented by Haidemenopoulos et al. [12] and extended in later studies introduces transformation kinetics equations for α′-Martensite formation under both stress-assisted and strain-induced conditions. This model has been integrated into homogenization frameworks for non-linear composite materials, allowing predictions of macroscopic mechanical behavior based on evolving phase fractions.

A physically based computational framework [2] (Fig. 2) was developed by Aristeidakis et al, to simulate the deformation behavior and transformation kinetics of austenitic steels under mechanical loading. The model begins by accepting key inputs such as alloy composition, temperature, and austenite grain size. Based on these parameters, it calculates the stacking fault energy (SFE), a critical factor governing the activation of deformation mechanisms such as mechanical twinning, ε-Martensite, and α′-Martensite formation. Following the SFE estimation, the model initializes the microstructure by defining the volume fractions of retained austenite, potential martensitic phases, and twins.

Institutional Repository - Library & Information Centre - University of Thessaly
13/09/2026 18:03:45 EEST - 216.73.216.14

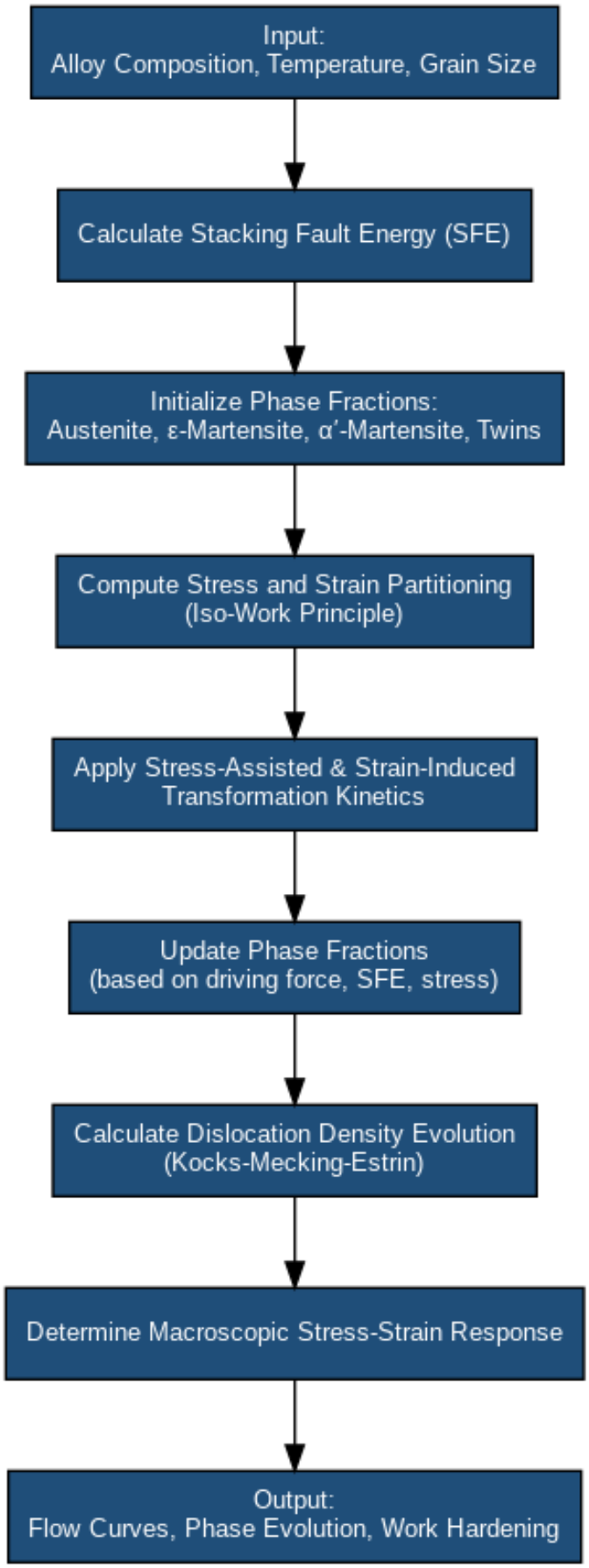

Fig. 2: Flow-chart of the austenite transformation kinetics model developed by John S. Aristeidakis

Stress and strain are then partitioned across the coexisting phases using the Iso-Work principle, ensuring mechanical compatibility during deformation. The model next applies both stress-assisted and strain-induced transformation kinetics, which are functions of SFE, applied stress, and strain history, to determine the evolution of phase fractions during loading. These updated phase fractions are used to calculate the dislocation density evolution via a modified Kocks-Mecking-Estrin [5,6,7,8] formulation that accounts for additional hardening due to martensite and twins.

Finally, the macroscopic mechanical response is determined, providing outputs such as true and nominal stress–strain curves, work-hardening rate, and transformation history of ε- and α′-Martensite. This stepwise methodology, implemented in MATLAB, enables the accurate prediction of steel behavior under cryogenic and mechanically demanding environments.

Importantly, these models incorporate critical parameters such as stacking fault energy (SFE), which governs the stability of retained austenite and the activation of either twinning or martensitic transformation. The ability to predict phase stability and transformation under varying temperature and strain conditions enables more efficient alloy design, particularly for cryogenic and energy-related applications.

Institutional Repository - Library & Information Centre - University of Thessaly
13/09/2026 18:03:45 EEST - 216.73.216.14

Chapter 3. Methodology

3.1 Modeling of the Stacking Fault Energy in Austenitic Steels

Modeling of the Stacking Fault Energy (SFE) of austenite in steels containing C, Mn, Al, Si, Ni, Cr and Mo was based on the work of John S. Aristeidakis and Gregory N. Haidemenopoulos [1]. Their MATLAB-based model utilizes the Olson-Cohen thermodynamic framework [3] to compute the SFE and estimate the interfacial energy ($\sigma^{\gamma\to\varepsilon}$), using an approximate solution developed by Pierce et al. [13]

3.1.1 Olson-Cohen Thermodynamic Model

The Olson-Cohen thermodynamic equation for the stacking fault energy Γ:

$$\Gamma = 2\rho\Delta G^{\gamma\to\varepsilon} + 2\sigma^{\gamma/\varepsilon}\ [J/m^2]$$

where:

- ρ: Molar surface density of atoms in the {1 1 1} planes based on Allain et al. [14]

  $$\rho = \frac{4}{\sqrt{3}\,a^2\,N}\ [mol/m^2]$$

  a: *Lattice parameter* [m]
  N: *Avogadro number* (6.022e23)

- $\Delta G^{\gamma\to\varepsilon}$: Free energy driving force for the $\gamma \to \varepsilon$ (FCC to HCP) transformation

  $$\Delta G^{\gamma\to\varepsilon} = \Delta G_{Ch}^{\gamma\to\varepsilon} + \Delta G_{Mag}^{\gamma\to\varepsilon} + \Delta G_{Ex}^{\gamma\to\varepsilon}\ [J/mol]$$

  $\boldsymbol{\Delta G_{Ch}^{\gamma\to\varepsilon}}$**:** Chemical contribution to the driving force

  $$\Delta G_{Ch}^{\gamma\to\varepsilon} = \sum_i X_i \Delta G_i^{\gamma\to\varepsilon} + X_{Fe}\sum_{i\neq Fe} X_i \Delta G_{Fe\ i}^{\gamma\to\varepsilon} + X_C X_{Mn} \Delta G_{C\ Mn}^{\gamma\to\varepsilon}$$

  where:
  $i = Fe, C, Mn, Al, Si, Ni, Cr, Mo$
  X_i *is the molar fraction of alloying element* i

Table. 3: Pure metal contributions and binary interaction terms in chemical driving force

Elements – Binary systems	$\boldsymbol{\Delta G_{Ch}^{\gamma\to\varepsilon}\ [J/mol]}$
Fe	$\Delta G_{Fe}^{\gamma\to\varepsilon} = -2243.38 + 4.309\,T$
C	$\Delta G_{C}^{\gamma\to\varepsilon} = -24595.12$
Mn	$\Delta G_{Mn}^{\gamma\to\varepsilon} = -1000 + 1.123\,T$
Al	$\Delta G_{Al}^{\gamma\to\varepsilon} = 5481.04 - 1.799\,T$
Si	$\Delta G_{Si}^{\gamma\to\varepsilon} = -560 - 8\,T$
Ni	$\Delta G_{Ni}^{\gamma\to\varepsilon} = 1046 + 1.2552\,T$
Cr	$\Delta G_{Cr}^{\gamma\to\varepsilon} = 1370 - 0.163\,T$
Mo	$\Delta G_{Mo}^{\gamma\to\varepsilon} = -3650 + 0.63\,T$
Fe-C	$\Delta G_{FeC}^{\gamma\to\varepsilon} = 42500$

Institutional Repository - Library & Information Centre - University of Thessaly
13/09/2026 18:03:45 EEST - 216.73.216.14

Fe-Mn	$\Delta G_{FeMn}^{\gamma\to\varepsilon} = 2873 - 717(X_{Fe} - X_{Mn})$
Fe-Al	$\Delta G_{FeAl}^{\gamma\to\varepsilon} = 3323$
Fe-Si	$\Delta G_{FeSi}^{\gamma\to\varepsilon} = 2850 + 3520(X_{Fe} - X_{Si})$
Fe-Ni	$\Delta G_{FeNi}^{\gamma\to\varepsilon} = 0$
Fe-Cr	$\Delta G_{FeCr}^{\gamma\to\varepsilon} = 2095$
Fe-Mo	$\Delta G_{FeMo}^{\gamma\to\varepsilon} = 0$
C-Mn	$\Delta G_{CMn}^{\gamma\to\varepsilon} = 26910$

$\boldsymbol{\Delta G_{Mag}^{\gamma\to\varepsilon}}$**:** Magnetic contribution to the driving force

Due to the paramagnetic to antiferromagnetic transition (FCC to HCP)

$$\Delta G_{Mag}^{\gamma\to\varepsilon} = G_{Mag}^{\varepsilon} - G_{Mag}^{\gamma}\ [J/mol]$$

$$G_{Mag}^{\varphi} = RT\ln\left(1 + \frac{\beta^{\varphi}}{\mu_B}\right) f\left(\frac{T}{T_N^{\varphi}}\right), \varphi = \gamma, \varepsilon$$

R: *Boltzmann constant*
T: *Temperature* $[K]$
β^{ε}: *Magnetic moment*
μ_B: *Bohr magneton*
T_N^{φ}*: Néel Temperature*, $\varphi = \gamma, \varepsilon$
$f\left(\frac{T}{T_N^{\varphi}}\right)$: Function given by Hillert et al. [15]
where:

$$\frac{\beta^{\gamma}}{\mu_B} = 0.7X_{Fe} + 0.62X_{Mn} - 0.64X_{Fe}X_{Mn} - 4X_C + 0.52X_{Ni} + 0.82X_{Cr}$$

$$\frac{\beta^{\varepsilon}}{\mu_B} = 0.62X_{Mn} - 4X_C + 0.52X_{Ni} + 0.82X_{Cr}$$

$$T_N^{\gamma} = -830.35X_C + 16228.644X_{Mn} - 5660.324(X_{Mn})\text{^}2 - 15583.508\ln(X_{Mn} + 1) - 787.447X_{Al} - 1254.734X_{Si} - 421.979X_{Ni} - 249.461X_{Cr} - 1325.711X_{Mo} + 149.863\ [K]$$

$$T_N^{\varepsilon} = 580X_{Mn} + 633X_{Ni} + 369.7X_{Cr}\ [K]$$

$\boldsymbol{\Delta G_{Ex}^{\gamma\to\varepsilon}}$**:** Excess energy term of the chemical driving force

$$\Delta G_{Ex}^{\gamma\to\varepsilon} = 170.06\exp\left(-\frac{d_{\gamma}}{18.55}\right)\ [J/mol]$$

d_{γ}*: Austenite particle diameter* [μm]

- $\sigma^{\gamma/\varepsilon}$: The interfacial energy approach by Pierce et al. [13]

$$\sigma^{\gamma/\varepsilon} = 10\left(2\rho\left(\Delta G_{Ch}^{\gamma\to\varepsilon} + \Delta G_{Mag}^{\gamma\to\varepsilon}\right)\right)^2 + 0.0095\ \ [J/m^2]$$

Institutional Repository - Library & Information Centre - University of Thessaly
13/09/2026 18:03:45 EEST - 216.73.216.14

3.1.2 MATLAB Implementation

The step-by-step methodology for calculating the SFE is illustrated in the flowchart that follows, detailing the sequence from alloy composition input to final SFE estimation, as implemented in a MATLAB-based simulation environment.

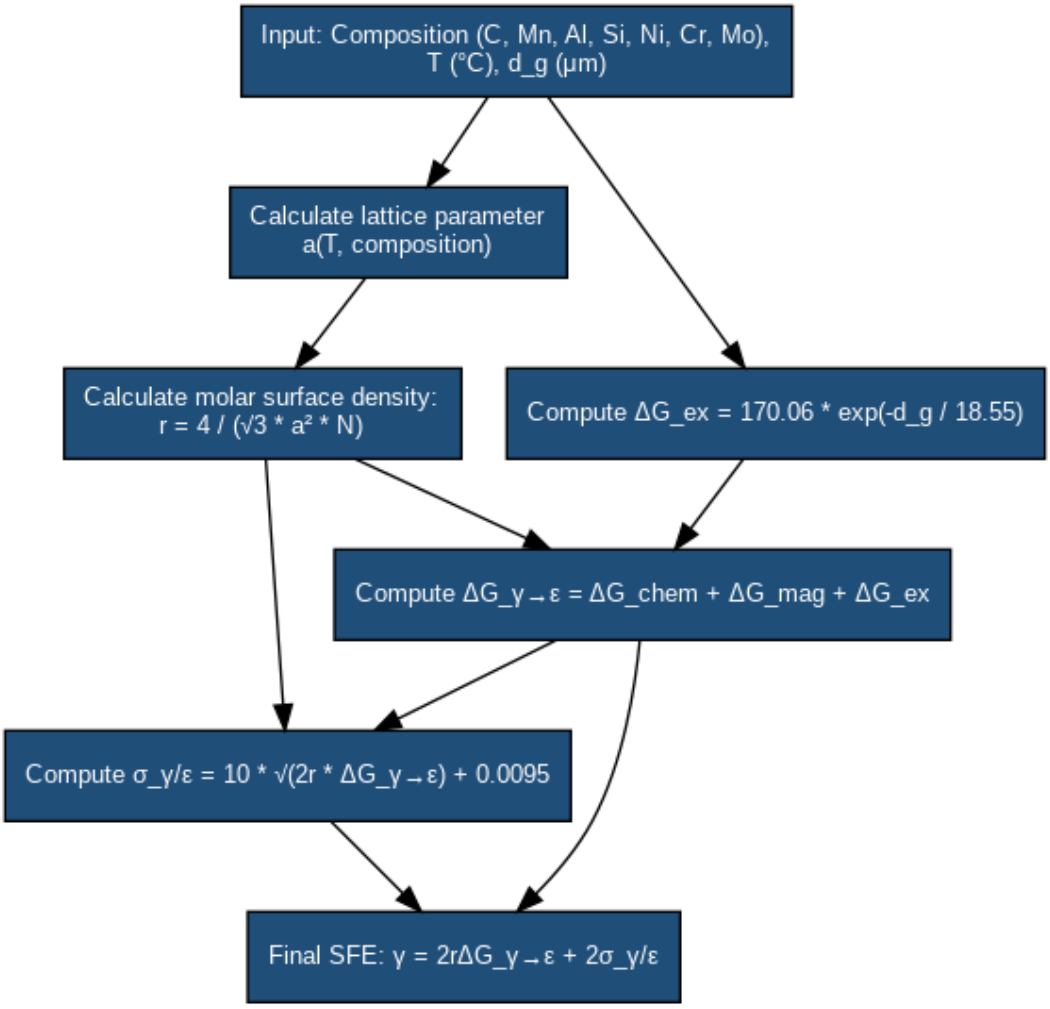

Fig. 3: Flowchart of the Stacking Fault Energy MATLAB implementation

The original model was appropriately modified to accept user-defined parameters as input, enabling flexible simulations based on multiple steel compositions and temperatures.

User Input Parameters

1. Austenite Composition (W)
   The user provides the weight percent composition of each alloying element in the austenite.

   The required input order is: C, Mn, Al, Si, Ni, Cr, Mo
   Input validation ensures that:

   - Each element's composition is between 0 and 100 wt.%
   - The total sum of all elements does not exceed 100%

Institutional Repository - Library & Information Centre - University of Thessaly
13/09/2026 18:03:45 EEST - 216.73.216.14

2. Austenite Temperature (T, in °C)
   Temperature is a required input to compute both SFE and $\sigma^{\gamma \rightarrow \varepsilon}$

   The user may:

   - Enter discrete temperature values
   - Define a temperature range ($T_{initial} \rightarrow T_{final}$) along with a step size for iterative calculations

3. Austenite Grain (Particle) Size (μm)
   The grain size input is needed to assess microstructural sensitivity and it is validated to ensure it is a positive value. Non-positive entries trigger appropriate handling or warnings.

```
>> Austenite_SFE
Enter the Austenite composition (%) in C: 0.0237
Enter the Austenite composition (%) in Mn: 7.018
Enter the Austenite composition (%) in Al: 0.0047
Enter the Austenite composition (%) in Si: 0.382
Enter the Austenite composition (%) in Ni: 4.07
Enter the Austenite composition (%) in Cr: 17.06
Enter the Austenite composition (%) in Mo: 0.0429

Type "Single" for single values of Temperature or "Range" for a selected range: Range
Enter initial Temperature in °C: 0
Enter final Temperature in °C: 20
Enter Temperature step: 10

Enter the austenite particle diameter dg in μm: 10

Stacking Fault Energy at 0°C = 0.019 J/m^2 = 19.43 mJ/m^2
Sigma = 0.010 J/m^2 = 9.91 mJ/m^2


_____________________________________________________________________________
Stacking Fault Energy at 10°C = 0.021 J/m^2 = 21.27 mJ/m^2
Sigma = 0.010 J/m^2 = 9.91 mJ/m^2


_____________________________________________________________________________
Stacking Fault Energy at 20°C = 0.023 J/m^2 = 23.10 mJ/m^2
Sigma = 0.010 J/m^2 = 9.91 mJ/m^2
```

Fig. 4: Command window of the Stacking Fault Energy MATLAB model

3.2 Modeling of the Stress Assisted and Strain Induced Transformation Kinetics

The second part of this thesis focuses on the martensitic transformation kinetics of austenitic stainless steels. Specifically, it examines the stress-strain response and phase transformation behavior of five well-known austenitic grades and a custom Duplex Stainless Steels: AISI 201, 304, 304L, 316 and 316L. The computational model, implemented in MATLAB, is also based on the foundational work of John S. Aristeidakis and Gregory N. Haidemenopoulos [2].

Institutional Repository - Library & Information Centre - University of Thessaly
13/09/2026 18:03:45 EEST - 216.73.216.14

The constitutive model is designed to simulate the mechanical behavior of steels containing metastable austenite under uniaxial tension. The methodology combines thermomechanical modeling with transformation kinetics to describe how retained austenite transforms into ε-Martensite, α′-Martensite, and mechanical twins during deformation, and how these evolving phases affect the stress–strain response of the material. The approach emphasizes the microstructural evolution as a function of strain, temperature, composition, and grain size.

1. Model Initialization

The simulation begins by defining the alloy's chemical composition, temperature, and austenite grain size, along with the initial volume fractions of all constituent phases—retained austenite, ferrite, δ-ferrite, and any pre-existing martensitic structures. These parameters influence austenite stability and are critical for predicting the likelihood and extent of transformation during loading.

2. Strain and Stress Partitioning

At each increment of applied strain, the model computes the total strain and stress in the material by combining the responses of all phases. This is done through weighted averaging, where each phase's contribution is scaled by its volume fraction. A key assumption in this process is the Iso-Work principle, which suggests that all phases undergo equal plastic work. This ensures realistic mechanical compatibility and energy balance between different microstructural regions.

$$\varepsilon = f_{\gamma}^{G} \cdot \varepsilon_{\gamma} + f_{\alpha'}^{G} \cdot \varepsilon_{\alpha'} + f_{\alpha}^{G} \cdot \varepsilon_{\alpha} + f_{\delta}^{G} \cdot \varepsilon_{\delta}$$

$$\sigma = (f_{\gamma}^{G} - f_{\varepsilon}^{G}) \cdot \sigma_{\gamma} + f_{\alpha'}^{G} \cdot \sigma_{\alpha'} + f_{\alpha}^{G} \cdot \sigma_{\alpha} + f_{\delta}^{G} \cdot \sigma_{\delta}$$

f_i^G: *Global volume fraction of phase*

ε_i: *Phase strain*

σ_i: *Phase stress*

where:

$i: \gamma - Austenite, \alpha' - Martensite, \varepsilon - Martensite, \alpha - Ferrite\ and\ \delta - Ferrite$

3. Phase-Specific Strain Behavior

In austenite, the total strain is divided into elastic, plastic, and transformation-induced components. Initially, if the applied stress is below the yield strength of austenite, only elastic and stress-assisted transformation strain are active. As the stress exceeds the yield threshold, plastic deformation initiates, and strain-induced mechanisms begin to prevail. The model accurately tracks this transition and estimates the hardening effects due to evolving microstructure.

Institutional Repository - Library & Information Centre - University of Thessaly
13/09/2026 18:03:45 EEST - 216.73.216.14

Austenite strain:

$$\varepsilon_\gamma = \varepsilon_\gamma^{el} + \varepsilon_\gamma^{pl} + \varepsilon_\gamma^{SA}$$

ε_γ^{el}: *Elastic strain of austenite*

ε_γ^{pl}: *Plastic strain of austenite*

ε_γ^{SA}: *Stress assisted transformation strain*

4. Transformation Kinetics

The formation of ε- and α′-Martensite, as well as mechanical twins, is governed by kinetic laws based on the material's stacking fault energy, composition, and temperature. Stress-assisted transformation occurs before yielding, triggered by local stress fields, while strain-induced transformation is activated after yielding and progresses with increasing plastic strain. These transformation mechanisms affect both the mechanical response and the phase stability during deformation.

Yield strength of austenite:

$$\sigma_\gamma^Y = \sigma_\gamma^0 + \sigma_\gamma^Y(\dot{\varepsilon}) + M_\gamma \cdot \alpha_{FH} \cdot \mu_\gamma \cdot b_\gamma \cdot \sqrt{\rho_\gamma}$$

Stress assisted transformation strain:

$$\varepsilon_\gamma^{SA} = f_\varepsilon^l \cdot \varepsilon_\varepsilon^{SA} + f_t^l \cdot \varepsilon_t^{SA}$$

where:

$$\varepsilon_\varepsilon^{SA} = \frac{2}{3} \cdot \varepsilon_\gamma^{SA}, \qquad \varepsilon_t^{SA} = \frac{1}{\sqrt{2}} M_\gamma$$

σ_γ^Y: $Austenite\ Yield\ stress\ [MPa]$

σ_γ^0: $Initial\ yield\ stress\ [MPa]$

$\sigma_\gamma^Y(\dot{\varepsilon})$: $Contribution\ to\ yield\ stress\ due\ to\ strain\ rate\ [MPa]$

M_γ: *Taylor factor*

α_{FH}: $Forest\ hardening\ coefficient$

μ_γ: $Shear\ modulus\ [MPa]$

b_γ: $Burgers\ vector\ [nm]$

ρ_γ: *Dislocation density in austenite* [m^{-2}]

$\varepsilon_\varepsilon^{SA}$: $Stress\ assisted\ transformation\ strain\ of\ \varepsilon - Martensite$

ε_t^{SA}: $Stress\ assisted\ transformation\ strain\ of\ mechanical\ twins$

Institutional Repository - Library & Information Centre - University of Thessaly
13/09/2026 18:03:45 EEST - 216.73.216.14

5. Dislocation Density and Hardening

As deformation proceeds, dislocations are generated and concentrated in the austenite and martensite phases. The model tracks this dislocation evolution using a physics-based law that balances dislocation generation (from grain boundaries, martensite/twin interfaces) and annihilation (through dynamic recovery). The dislocation density directly influences the flow stress and the material's strain-hardening behavior, allowing the model to capture the increase in strength with strain realistically.

Dislocation density increase rate:

$$\frac{\partial \rho_\gamma}{\partial \varepsilon} = \frac{M_\gamma}{b_\gamma}\left(\frac{P_\gamma}{D_\gamma} + \sum \frac{1}{\Lambda_i} + k_1^\gamma \cdot \sqrt{\rho_\gamma} - f_{DRV}^\gamma \cdot b_\gamma \cdot \rho_\gamma\right)$$

P_γ: $Dislocation\ source\ factor$

D_γ: $Austenite\ grain\ size\ [\mu m]$

Λ_i: $Dislocation\ free\ mean\ path\ [m]$

k_1^γ: $Dislocation\ generation\ factor$

f_{DRV}^γ: $Dynamic\ recovery\ coefficient$

6. Numerical Solution

The simulation uses an explicit Euler integration method to solve the system of equations incrementally describing the mechanical and microstructural evolution. At each step of strain, the model updates the stress, strain, dislocation density, and phase fractions. This iterative process continues until the desired total strain is reached, producing a full stress–strain curve.

7. Output and Interpretation

The model output includes:

- **True and nominal stress–strain curves**, showing the material's macroscopic response.
- **Volume fraction evolution** of ε-Martensite, α′-Martensite, and twins as functions of strain.
- **Work-hardening rate**, offering insights into the deformation mechanisms.
- **Dislocation density trajectories** for each phase.

The original model was tailored to incorporate these five alloys as predefined simulation options at various temperatures and values of the austenite particle diameter (D_g) in μm, and test their elastoplastic response as well as determine the volume fractions of stress assisted (SA) and strain induced (SI) ε-, α'-Martensite and twinning.

Institutional Repository - Library & Information Centre - University of Thessaly
13/09/2026 18:03:45 EEST - 216.73.216.14

In alignment with the objectives of this research, five major austenitic steels and Duplex stainless steel were tested as the most suitable candidates for liquified fuel storage applications at cryogenic temperatures. The MATLAB script was adjusted to include their corresponding alloying element concentrations (W_g), allowing the user to automatically select a steel grade by entering a number (1–5) in the command window. The temperature (T) and austenite particle diameter (D_g) are also required inputs to define transformation conditions.

Additionally, the user has the option to modify five key material parameters:

- **Initial nucleation site density for stress-assisted transformation (N_0^{SA})**
- **Dislocation generation factors** for both γ-austenite and α′-Martensite **(k_1^{γ}, $k_1^{\alpha'}$)**
- **Dynamic recovery coefficients ($f_{DRV_0}^{\gamma}$, $f_{DRV}^{\alpha'}$)**
- **Hall–Petch strengthening coefficient of austenite (k_{γ}^{HP})**
- **Initial dislocation densities (ρ_{γ}^{0}, $\rho_{\alpha'}^{0}$)**

Default values are assigned if the user does not specify changes.

Moreover, a custom alloy composition can be used by entering a dash (-) in the command prompt. In this case, the user is prompted to specify the global volume fraction of austenite (0–1). If the value is less than 1, additional input is required for the α-ferrite composition (W_aF) and particle diameter (D_aF).

```
>> Main_Code
Austenitic Stainless Steels
1. AISI 201.. 0.0237C - 7.018Mn - 0.0047Al - 0.382Si - 4.07Ni - 17.06Cr - 0.0429Mo - 0.164N
2. 304..... 0.08C - 2Mn - 0.04Al - 0.75Si - 8Ni - 18Cr - 0Mo - 0.1N
3. 304L..... 0.03C - 2Mn - 0.04Al - 0.75Si - 9Ni - 18Cr - 0Mo - 0.1N
4. 316..... 0.08C - 2Mn - 0.04Al - 0.75Si - 10.5Ni - 17.5Cr - 2.5Mo - 0.1N
5. 316L..... 0.03C - 2Mn - 0.04Al - 0.75Si - 10Ni - 16Cr - 2Mo - 0.1N

Enter the number of the Austenitic SS alloy or press "-" to enter a specific composition: -
Enter the Austenite composition (%) in C: 0.02
Enter the Austenite composition (%) in Mn: 8
Enter the Austenite composition (%) in Al: 0.005
Enter the Austenite composition (%) in Si: 0.3
Enter the Austenite composition (%) in Ni: 4
Enter the Austenite composition (%) in Cr: 18
Enter the Austenite composition (%) in Mo: 0.04
Enter the Austenite composition (%) in N: 0.1

Enter the initial volume fraction of Austenite (0-1): 1


Enter the Austenitic steel Temperature in °C: 20

Enter the austenite particle diameter D_g in μm: 10

Would you like to set new values to the input parameters of the system?
Default values will be used alternatively (yes or no): yes
Enter the initial nucleation site density for the SA transformation (Default value = 17.193e18 1/m³): 16e18

Austenite Input Parameters
Enter the Austenite dislocation generation factor (Default value = 0.05319): 0.052
Enter the Austenite dynamic recovery coefficient constant (Default value = 38.812): 39
Enter the Austenite Hall-Petch strengthening coefficient (Default value = 500 MPa μm^½): 500
Enter the initial dislocation density of Austenite (Default value = 5e13 1/m²): 5e13

a'-Martensite Input Parameters
Enter the a'-Martensite dislocation generation factor (Default value = 0.1): 0.1
Enter the a'-Martensite dynamic recovery coefficient constant (Default value = 3.5879): 3.6
Enter the initial dislocation density of a'-Martensite (Default value = 1e15 1/m²): 1e15
```

Fig. 5: Command window of the martensitic transformation model implemented in MATLAB

Institutional Repository - Library & Information Centre - University of Thessaly
13/09/2026 18:03:45 EEST - 216.73.216.14

Chapter 4. Results and Discussion

The results of the application of the aforementioned methodology to the five austenitic alloys are presented below.

4.1 AISI 201 austenitic stainless steel

The investigated steel grade was initially fully austenitic, with a nominal composition of 0.0237% C, 7.018% Mn, 0.0047% Al, 0.382% Si, 4.07% Ni, 7.06% Cr, 0.0429% Mo, and 0.164% N by mass, as illustrated in Fig. 6a. The deformation behavior of the material at 20 °C involved both stress-assisted and strain-induced transformation mechanisms, resulting in the progressive formation of ε-Martensite, α′-Martensite, and mechanical twins.

At this temperature, the stacking fault energy and interfacial energy of austenite were determined using the computational model as:

$$\gamma_{SFE} = 11.1733\, mJ/m^2, \quad \sigma_{\gamma/\varepsilon} = 11.8771\, mJ/m^2$$

These values indicate a low stacking fault energy regime, which promotes both TRIP (Transformation-Induced Plasticity) and TWIP (Twinning-Induced Plasticity) effects. As applied strain increases, the austenite phase becomes unstable and progressively transforms, activating these mechanisms.

The effect of the TRIP and TWIP phenomena is evident in the work-hardening behavior, shown in Fig. 6c, where a clear hump is observed in the $\frac{d\sigma}{d\varepsilon}$ curve around a true strain of 0.2. This behavior corresponds to the sudden increase in α′-Martensite content, enhancing the material's strength and work-hardening rate. Simultaneously, the phase evolution plot (Fig. 6a) reveals a sharp increase in martensite volume fraction, coinciding with the onset of the stress–strain plateau observed in Fig. 6b. At this point, retained austenite rapidly transforms, causing its curve to decline sharply while the martensite curve rises. This transformation sequence illustrates the dual contribution of TWIP and TRIP effects to the material's deformation resistance. Twins and ε-Martensite contribute during early deformation stages, while α′-Martensite formation dominates at higher strains. The interaction between these mechanisms is responsible for the observed strain hardening and the strength–ductility synergy characteristic of metastable austenitic steels under cryogenic or near-room-temperature values.

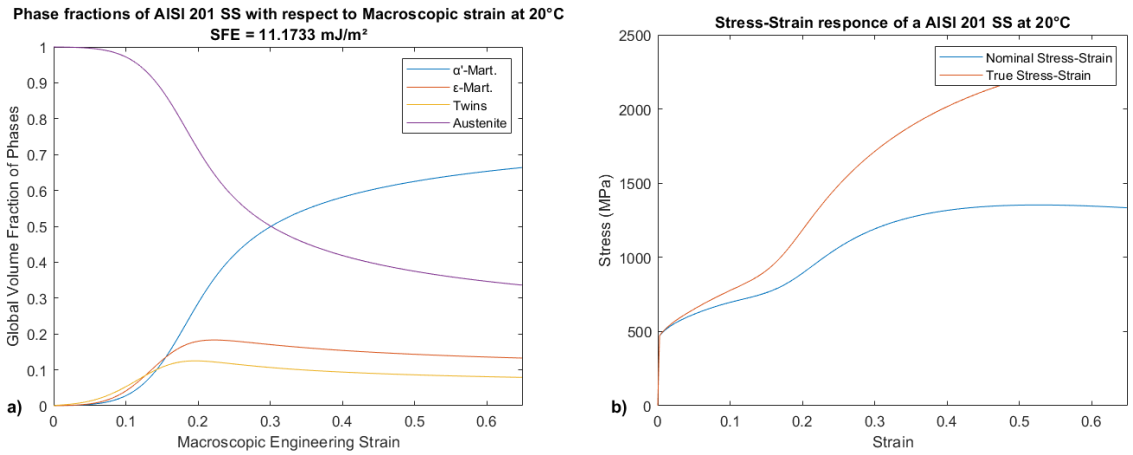

Institutional Repository - Library & Information Centre - University of Thessaly
13/09/2026 18:03:45 EEST - 216.73.216.14

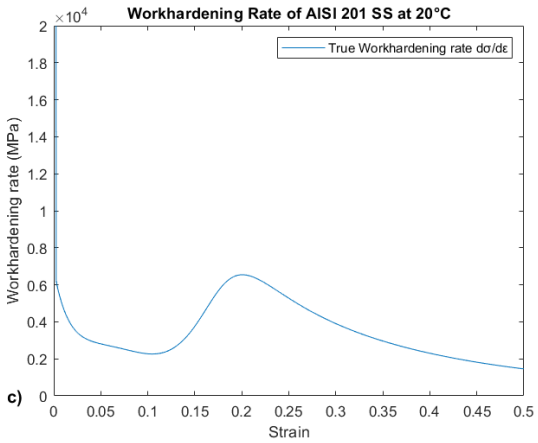

Fig. 6: AISI 201 response to applied mechanical strain. The phase fraction evolution (a) from fully to partially austenitic due to martensitic transformation. The computed stress-strain response (b) and the work-hardening rate (c) with respect to true strain

The influence of two critical microstructural parameters-temperature and austenite grain (particle) size-on the transformation kinetics of stress-assisted (SA) and strain-induced (SI) α′-Martensite was investigated using a series of physically based numerical simulations. These simulations were implemented in MATLAB using a constitutive model developed for steels containing retained austenite. The objective was to quantify the role of these variables on both the volume fraction of α′-Martensite and the overall elastoplastic response of the material.

To evaluate the effect of temperature, simulations were conducted across a range of sub-zero to ambient temperatures, specifically from –80 °C to 20 °C, representative of cryogenic storage conditions. The simulation results, depicted in Fig. 7a, indicate that lowering the temperature enhances the transformation of austenite into α′-Martensite at lower strain levels, with the phase fraction approaching unity ($f_{\alpha'} \rightarrow 1$). This trend is related to the reduction of Stacking Fault Energy (SFE) at lower temperatures, which decreases the mechanical stability of austenite and facilitates earlier onset of martensitic transformation.

This transformation behavior is mirrored in the stress–strain response shown in Fig. 7c. As the temperature decreases, higher tensile stresses are required to achieve the same level of nominal strain. This is consistent with increased strain hardening caused by enhanced martensite formation and mechanical twinning at cryogenic temperatures.

The effect of austenite grain size on the formation of α′-Martensite was also examined by varying the austenite particle diameter from 5 μm to 40 μm. As illustrated in Fig. 7b, an increase in grain size results in a notable rise in the global volume fraction of α′-Martensite. This phenomenon is explained by the reduction in grain boundary area in coarse-grained microstructures, which lowers the barrier to martensite nucleation and growth. As a result, the mechanical stability of retained austenite decreases with increasing grain size, favoring transformation.

Together, these results highlight the sensitivity of TRIP kinetics to both temperature and microstructure and underscore the importance of optimizing processing parameters to tailor the transformation behavior and mechanical performance of austenitic steels for applications under extreme environmental conditions.

Institutional Repository - Library & Information Centre - University of Thessaly
13/09/2026 18:03:45 EEST - 216.73.216.14

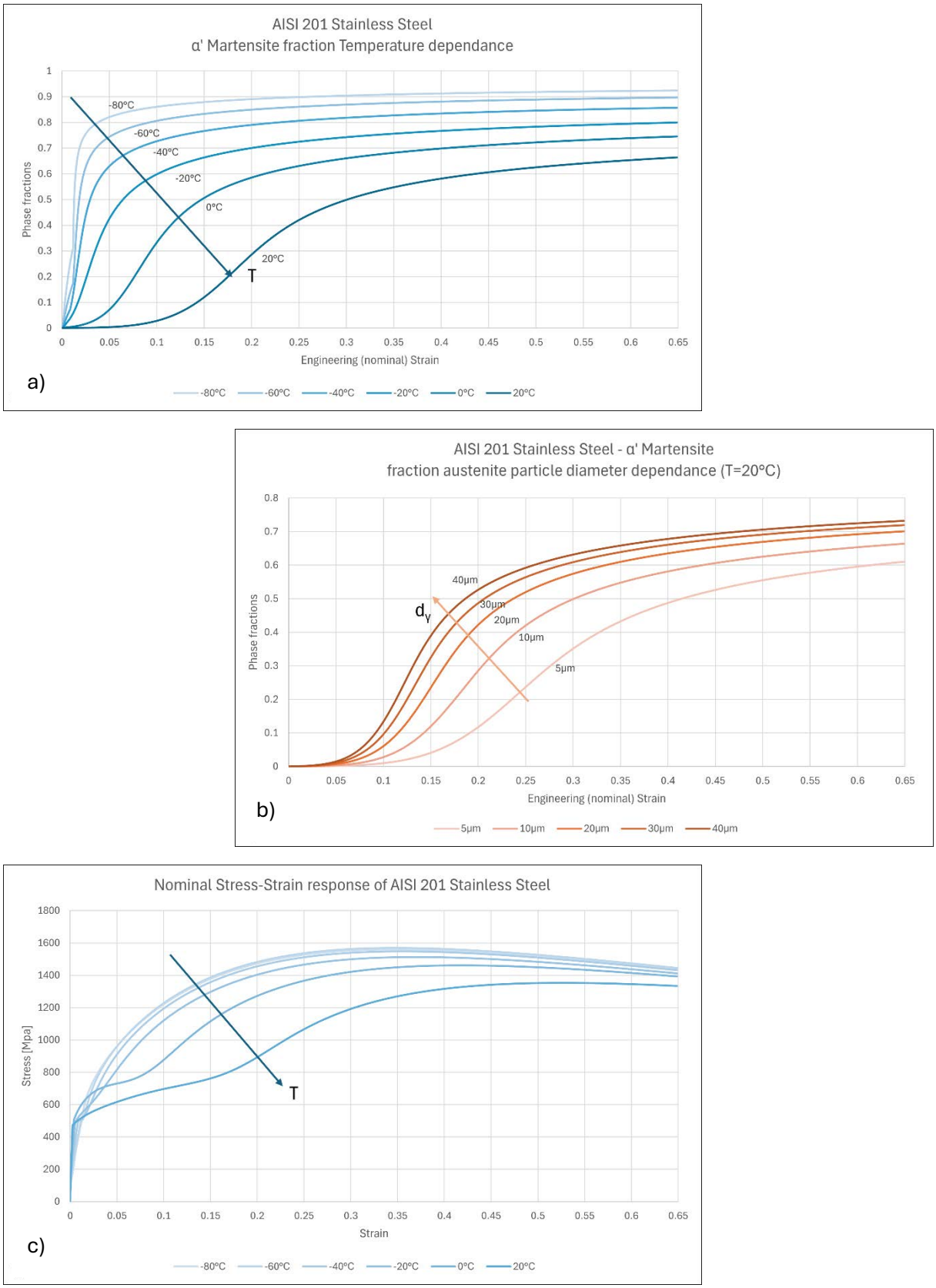

Fig. 7: AISI 201 sensitivity to constitutive model parameters. α'-Martensite volume phase fraction (a) correlation with temperature and (b) austenite grain diameter and the alloy's nominal stress-strain response (c) at various temperature values

Institutional Repository - Library & Information Centre - University of Thessaly
13/09/2026 18:03:45 EEST - 216.73.216.14

4.2 AISI 304 austenitic stainless steel

The steel grade examined in this simulation was fully austenitic AISI 304, with a nominal composition of 0.08% C, 2% Mn, 0.04% Al, 0.75% Si, 8% Ni, 18% Cr, and 0.1% N by mass. This composition represents a stable austenitic phase under ambient conditions.

At a temperature of 20 °C, the computational model yielded a stacking fault energy of:

$$\gamma_{SFE} = 12.5549\ mJ/m^2$$

and an interfacial energy of:

$$\sigma_{\gamma/\varepsilon} = 11.5509\ mJ/m^2$$

quantifying the austenite's resistance to ε-martensitic transformation.

The transformation kinetics of AISI 304 were found to be qualitatively similar to those of AISI 201, showing activation of stress-assisted and strain-induced martensitic transformation mechanisms under applied strain. Additionally, the elastoplastic behavior—including the shape of the stress–strain curve and the work hardening rate—followed the same trends observed in AISI 201. This suggests that while AISI 304 may exhibit slightly higher stacking fault energy, its mechanical response and phase stability characteristics at room temperature still permit notable TRIP effects under appropriate conditions.

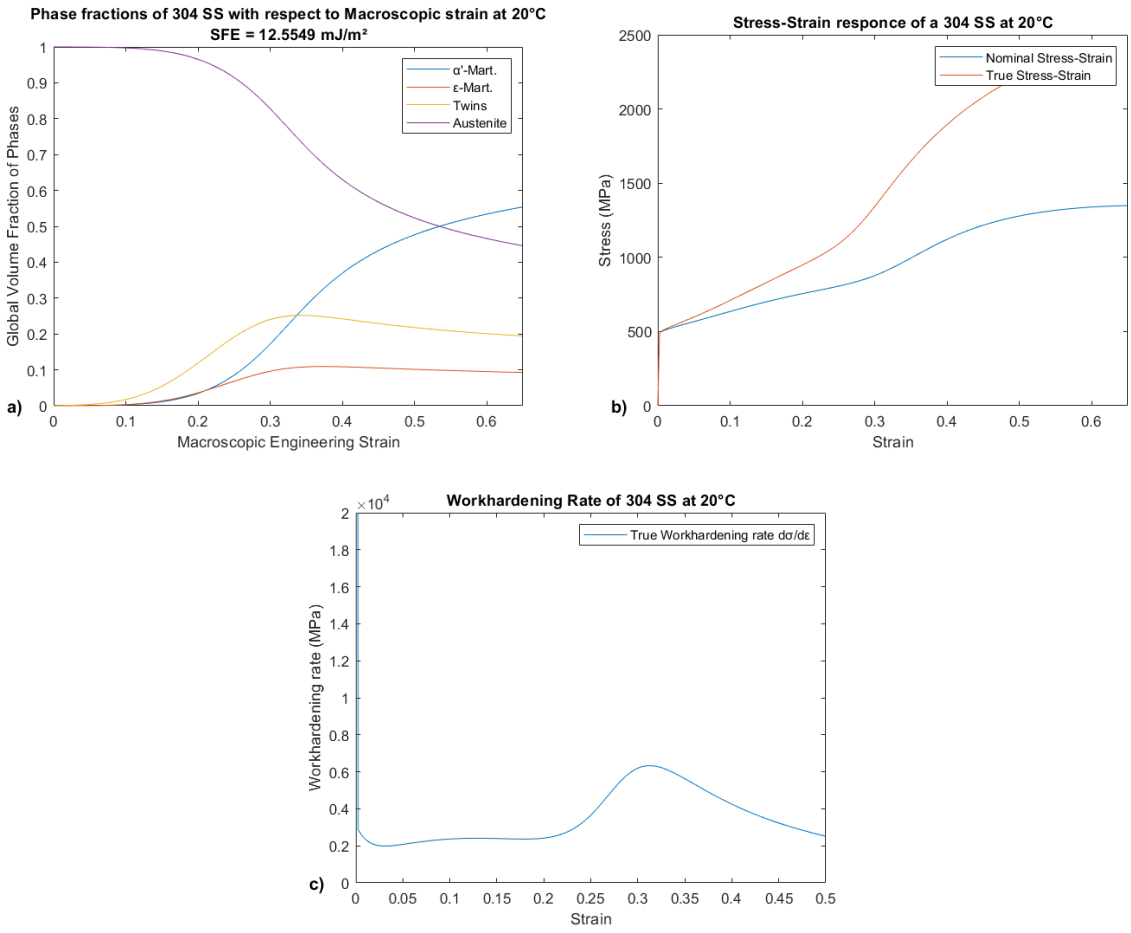

Fig. 8: AISI 304 response to applied mechanical strain. The phase fraction evolution (a) from fully to partially austenitic due to martensitic transformation. The computed stress-strain response (b) and the work-hardening rate (c) with respect to true strain

Institutional Repository - Library & Information Centre - University of Thessaly
13/09/2026 18:03:45 EEST - 216.73.216.14

The same applies to the temperature and austenitic grain size dependance of α'-Martensite as well as its mechanical response in cryogenic conditions.

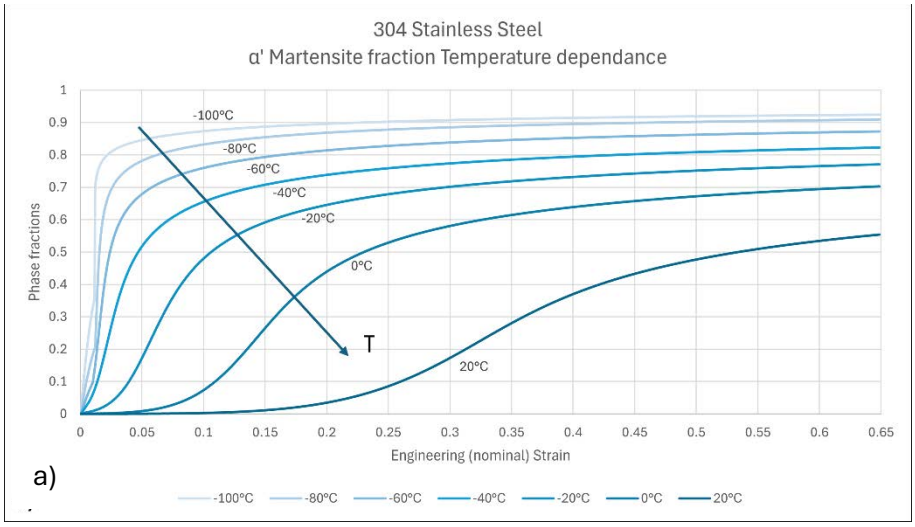

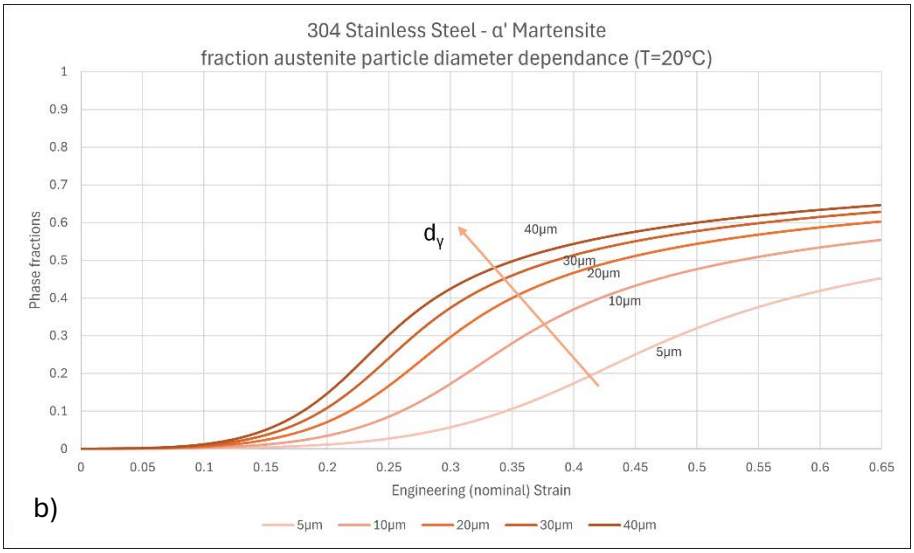

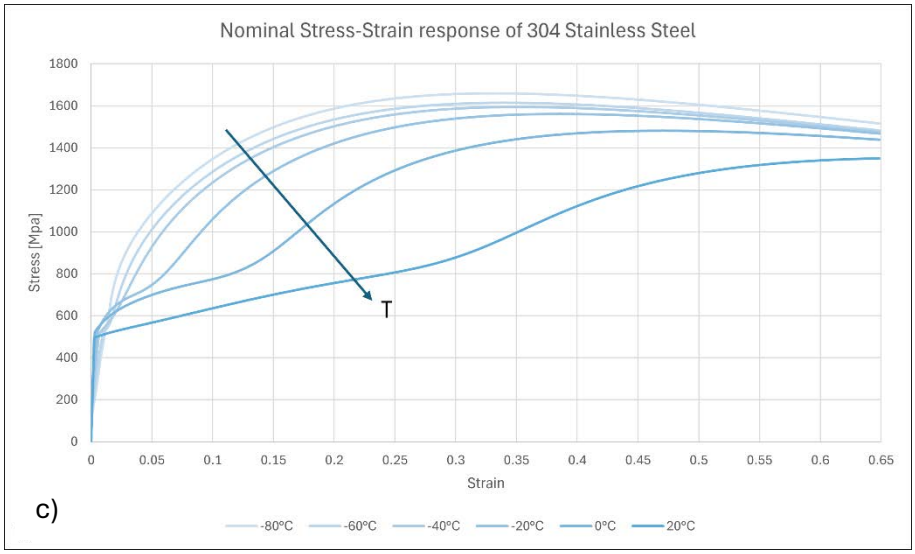

Fig. 9: AISI 304 sensitivity to constitutive model parameters. α'-Martensite volume phase fraction (a) correlation with temperature and (b) austenite grain diameter and the alloy's nominal stress-strain response (c) at various temperature values

Institutional Repository - Library & Information Centre - University of Thessaly
13/09/2026 18:03:45 EEST - 216.73.216.14

4.3 AISI 304L stainless steel

Composition: 0.03% C, 2% Mn, 0.04% Al, 0.75% Si, 9% Ni, 18% Cr and 0.1% N

$$\gamma_{SFE} = 12.9161\ mJ/m^2\ , \quad \sigma_{\gamma/\varepsilon} = 11.4992\ mJ/m^2 \text{ at } 20^oC$$

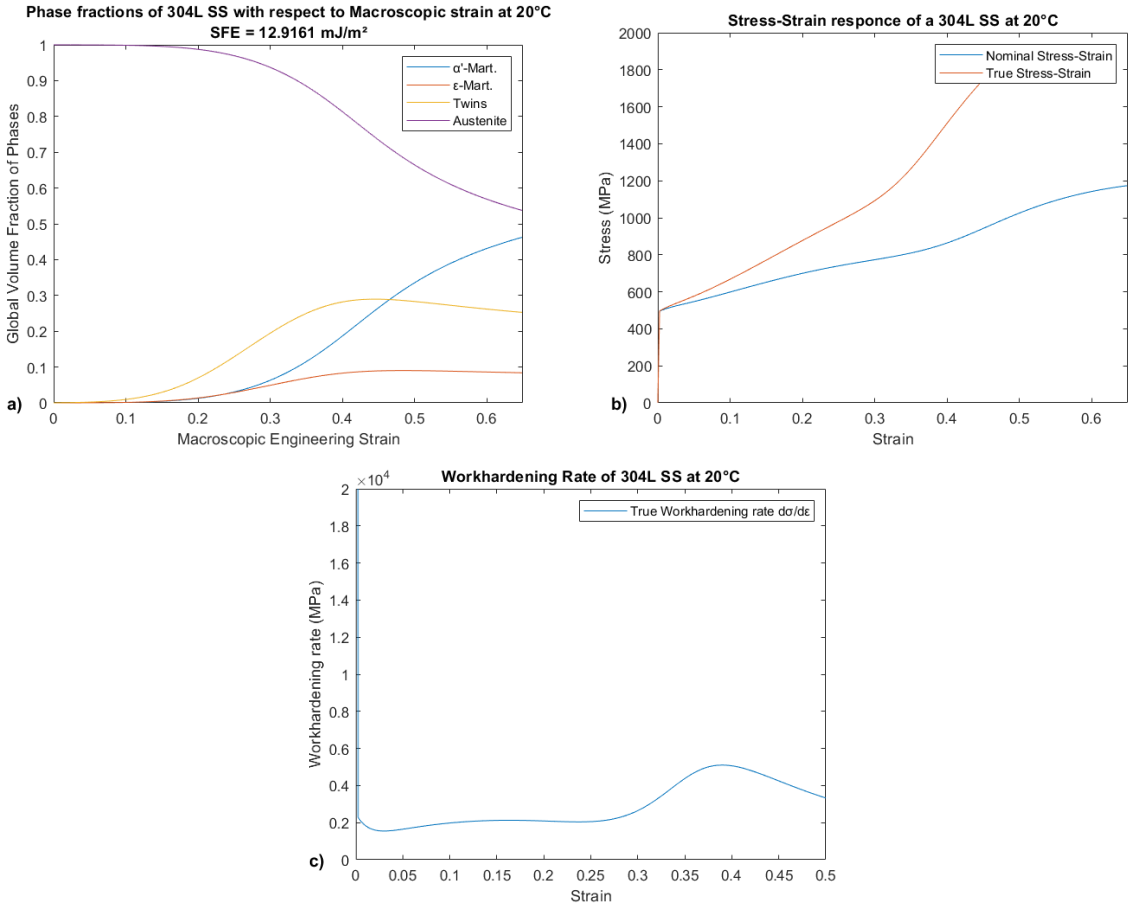

Fig. 10: AISI 304L response to applied mechanical strain. The phase fraction evolution (a) from fully to partially austenitic due to martensitic transformation. The computed stress-strain response (b) and the work-hardening rate (c) with respect to true strain

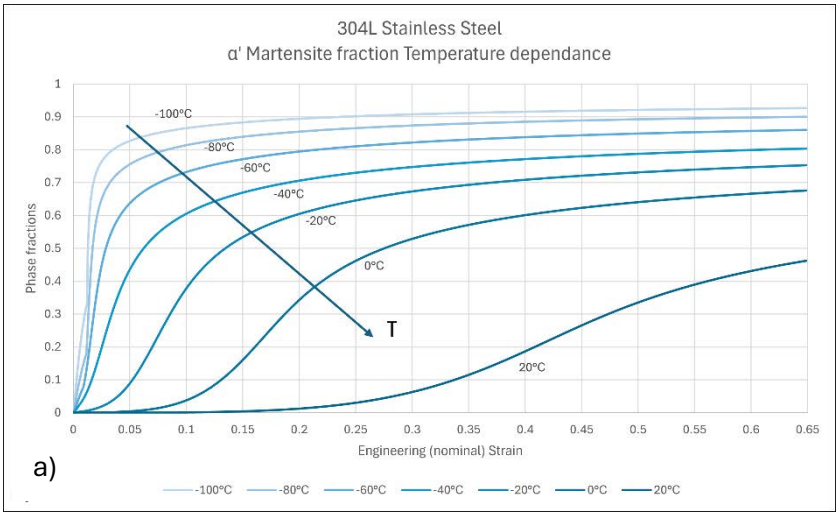

Fig. 11: AISI 304L sensitivity to constitutive model parameters. α'-Martensite volume phase fraction (a) correlation with temperature

Institutional Repository - Library & Information Centre - University of Thessaly
13/09/2026 18:03:45 EEST - 216.73.216.14

4.4 AISI 316 stainless steel

Composition: 0.08% C, 2% Mn, 0.04% Al, 0.75% Si, 10.5% Ni, 17.5% Cr, 2.5% Mo and 0.1% N

$$\gamma_{SFE} = 12.1120\ mJ/m^2, \quad \sigma_{\gamma/\varepsilon} = 11.6073\ mJ/m^2 \text{ at } 20^{o}\text{C}$$

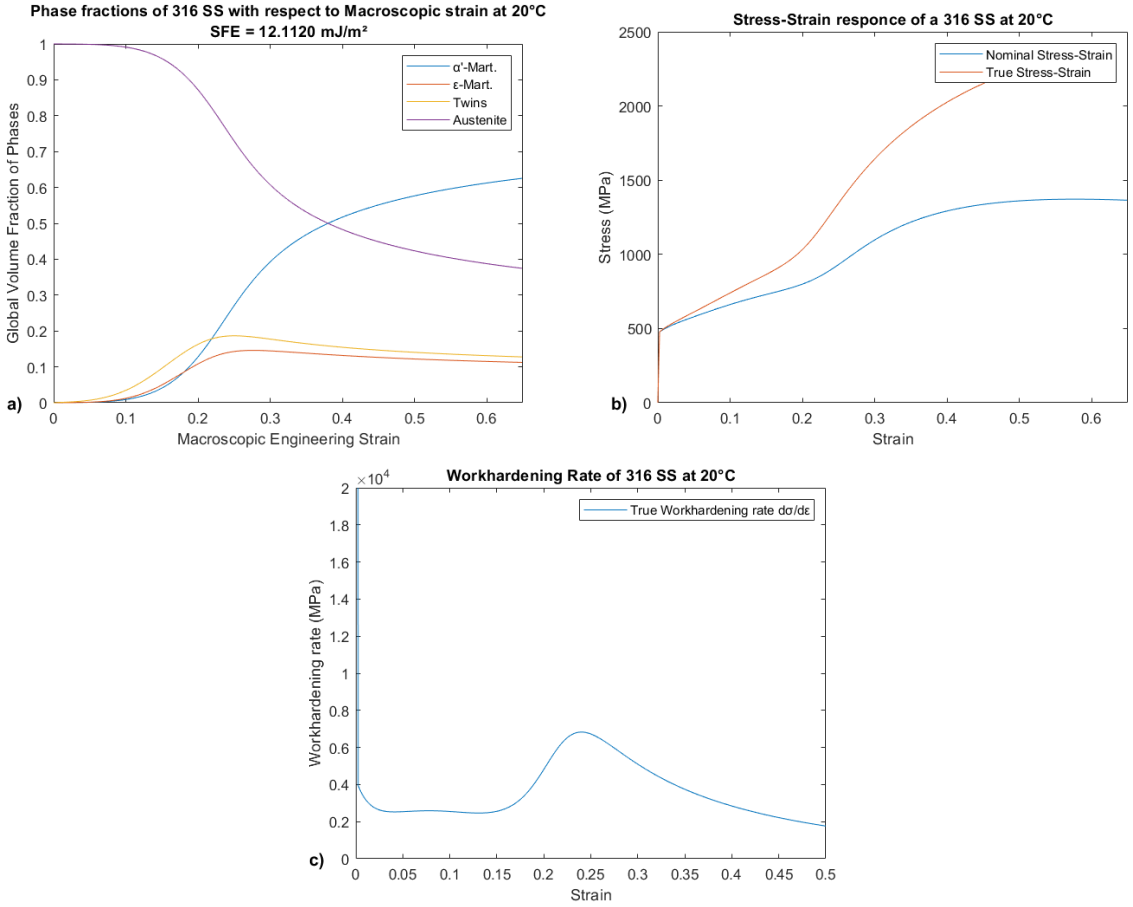

Fig. 12: AISI 316 response to applied mechanical strain. The phase fraction evolution (a) from fully to partially austenitic due to martensitic transformation. The computed stress-strain response (b) and the work-hardening rate (c) with respect to true strain

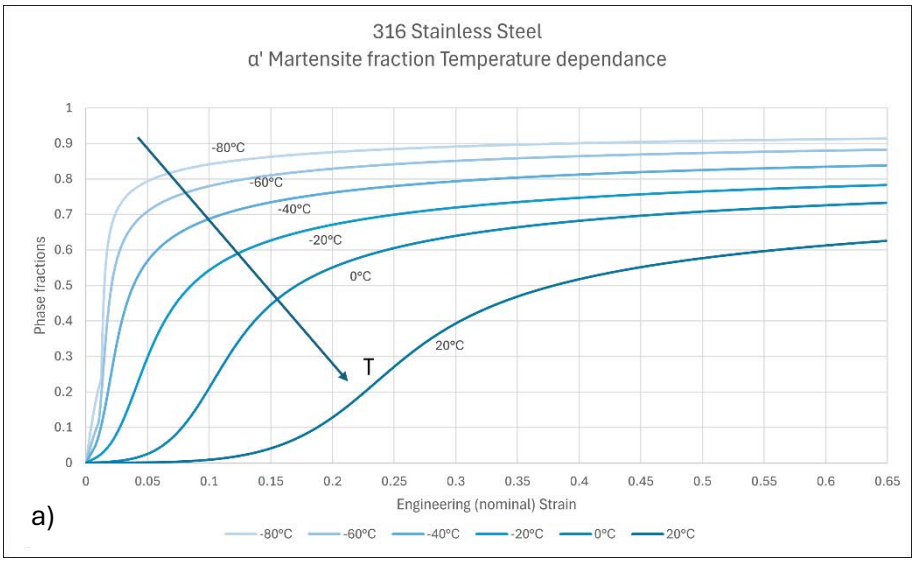

Fig. 13: AISI 316 sensitivity to constitutive model parameters. α'-Martensite volume phase fraction (a) correlation with temperature

Institutional Repository - Library & Information Centre - University of Thessaly
13/09/2026 18:03:45 EEST - 216.73.216.14

4.5 AISI 316L stainless steel

Composition: 0.03% C, 2% Mn, 0.04% Al, 0.75% Si, 10% Ni, 16% Cr, 2% Mo and 0.1% N

$$\gamma_{SFE} = 10.4005\ mJ/m^2, \quad \sigma_{\gamma/\varepsilon} = 12.1275\ mJ/m^2 \text{ at } 20^{o}\text{C}$$

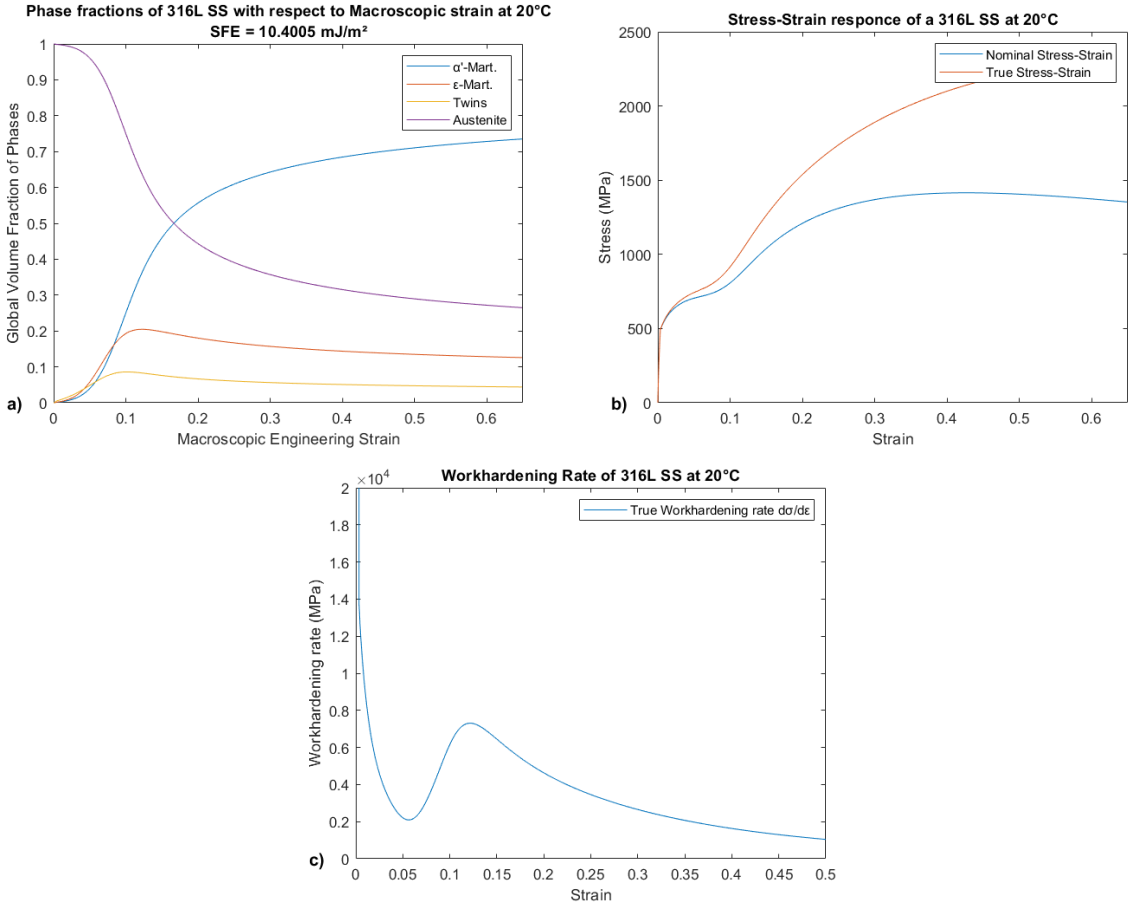

Fig. 14: AISI 316L response to applied mechanical strain. The phase fraction evolution (a) from fully to partially austenitic due to martensitic transformation. The computed stress-strain response (b) and the work-hardening rate (c) with respect to true strain

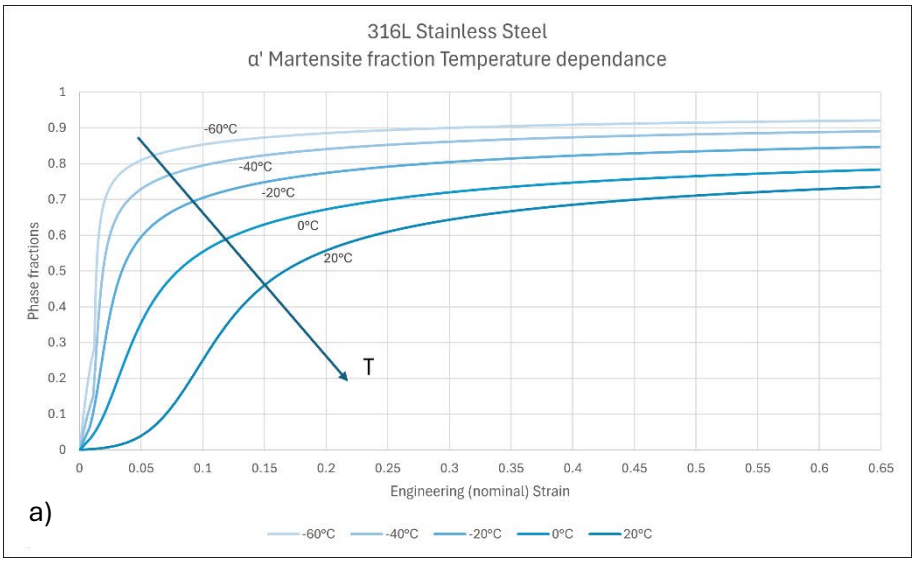

Fig. 15: AISI 316L sensitivity to constitutive model parameters. α'-Martensite volume phase fraction (a) correlation with temperature

Institutional Repository - Library & Information Centre - University of Thessaly
13/09/2026 18:03:45 EEST - 216.73.216.14

4.6 Duplex Stainless Steel

The final alloy evaluated in this study was a custom duplex stainless steel compositionally and structurally similar to commercial Duplex 2205 (UNS S32205), a two-phase material comprising both ferrite and austenite. The initial global phase volume fractions were set as 65% austenite $f_\gamma^G = 0.65$ and 35% ferrite $f_\alpha^G = 0.35$, respectively. The austenitic phase had a nominal composition of 0.025% C, 1.5% Mn, 0.005% Al, 0.3% Si, 9% Ni, 21.5% Cr, 3.2% Mo, and 0.3% N by mass, while the ferritic phase contained 0.002% C, 0.8% Mn, 0.005% Al, 0.4% Si, 3.5% Ni, 26% Cr, 3% Mo, and 0.08% N. The resulting global composition of the alloy was calculated to be 0.017% C, 1.25% Mn, 0.005% Al, 0.34% Si, 7.52% Ni, 23.78% Cr, 3.12% Mo, and 0.23% N.

This duplex alloy is currently employed in the cryogenic storage of liquefied natural gas (LNG), where both mechanical robustness and phase stability at sub-zero temperatures are crucial. At 20 °C, the stacking fault energy of the austenite phase and the associated interfacial energy were calculated to be:

$$\gamma_{SFE} = 14.537\ mJ/m^2, \quad \sigma_{\gamma/\varepsilon} = 11.4\ mJ/m^2$$

Among all the alloys investigated in this study, this value of stacking fault energy is the highest at ambient temperature, indicating a relatively stable austenitic phase less prone to transformation into ε- or α′-Martensite. This enhanced stability suggests reduced TRIP activity and more uniform deformation, both of which are desirable traits for materials operating under cryogenic service conditions.

The mechanical response of the Duplex stainless steel under applied strain at 20 °C is mostly consistent with the behavior observed in the fully austenitic alloys previously analyzed. However, a key distinction lies in the initial microstructural composition: the austenite phase constitutes only 65% of the total volume. As a result, the maximum possible volume fraction of α′-Martensite formed through transformation is inherently limited to this initial austenite fraction. This upper bound is clearly reflected in Fig. 16a, where the α′-Martensite curve asymptotically approaches a value significantly below 0.65 as strain increases.

The phase transformation proceeds gradually, with notable activation of both ε-Martensite and mechanical twinning before the onset of α′-Martensite, which becomes more pronounced beyond a nominal strain of approximately 0.25. The evolution of these phases corresponds with the stress–strain behavior shown in Fig. b, which reveals a moderate hardening rate and smooth curve progression. The alloy exhibits a stable plastic deformation regime without abrupt stress jumps, suggesting controlled transformation kinetics and limited instability. This behavior is consistent with its relatively high stacking fault energy, which results in dislocation glide and delays phase transformation, thereby preserving ductility under strain.

Institutional Repository - Library & Information Centre - University of Thessaly
13/09/2026 18:03:45 EEST - 216.73.216.14

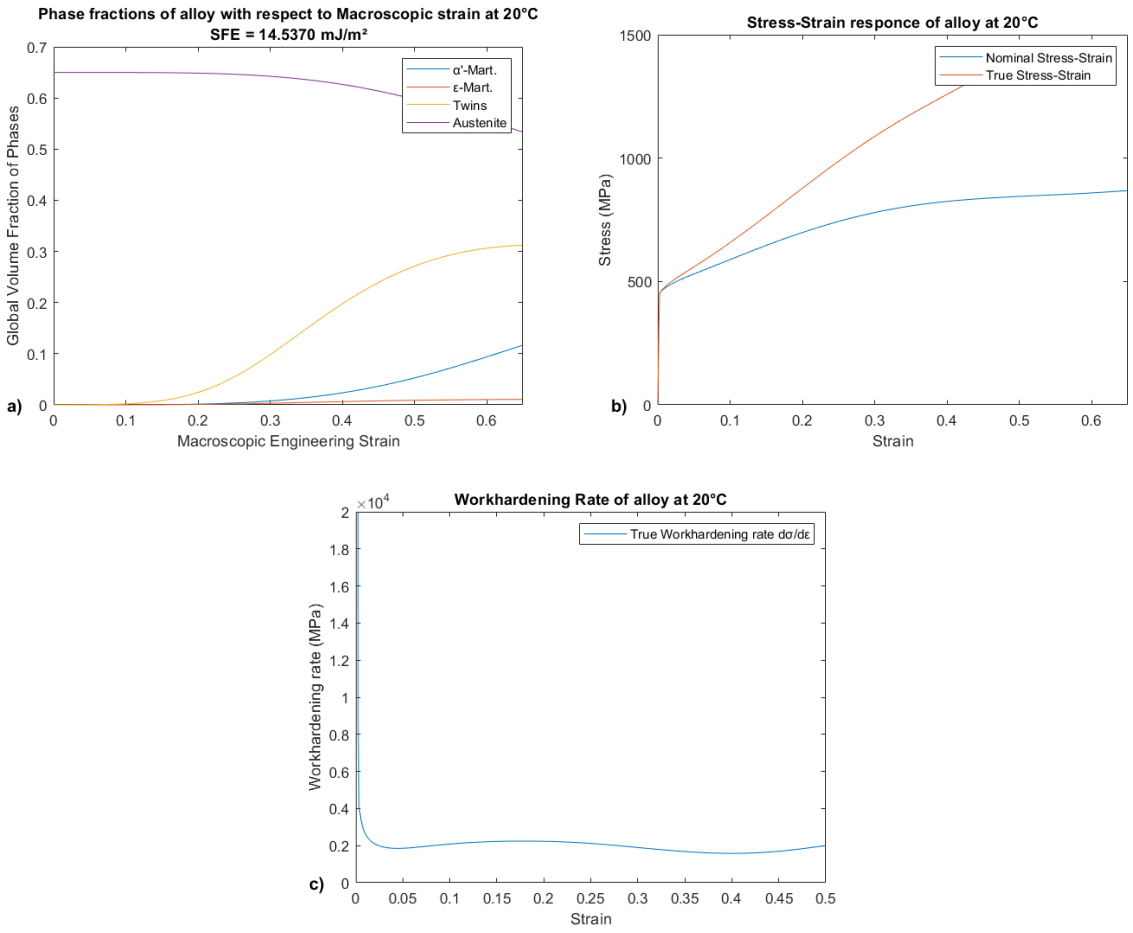

Fig. 16: Duplex SS response to applied mechanical strain. The phase fraction evolution (a) from 65% austenitic to partially austenitic due to martensitic transformation. The computed stress-strain response (b) and the work-hardening rate (c) with respect to true strain

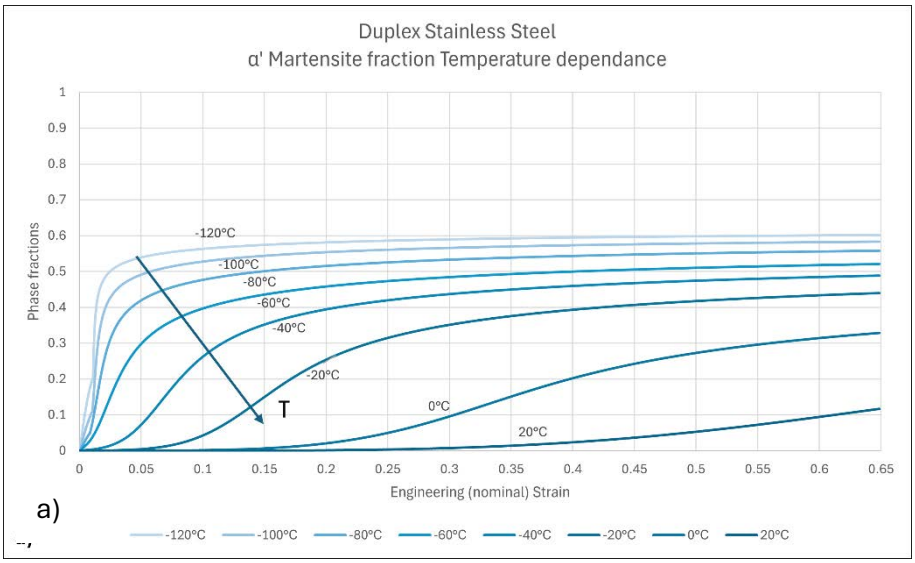

Fig. 17: Duplex SS sensitivity to constitutive model parameters. α'-Martensite volume phase fraction (a) correlation with temperature

Institutional Repository - Library & Information Centre - University of Thessaly
13/09/2026 18:03:45 EEST - 216.73.216.14

4.7 Performance Evaluation

To evaluate the performance of the studied stainless steels under tensile loading, a comparative assessment was conducted using three key indicators derived from numerical simulations:

1. the **evolution of martensite volume fraction**
2. the **stress–strain response**
3. the **work-hardening rate** $\left(\frac{d\sigma}{d\varepsilon}\right)$

Together, they provide a comprehensive view of both the transformation kinetics and the mechanical behavior of each alloy. The final volume fraction of α′-Martensite reflects the austenite phase stability and the extent of stress- or strain-induced transformation. The stress–strain curves provide insight into yield strength, uniform elongation, and the overall ductility of the material. Additionally, the work-hardening rate curve captures the dynamic strengthening mechanisms active during deformation, including the onset and evolution of the TRIP and TWIP effects. By analyzing these parameters collectively, the alloys can be ranked according to their transformation resistance, deformation capacity, and suitability for applications that require a combination of strength and ductility, such as cryogenic fuel storage.

Table. 4: Data retrieved by the study and their use for the candidates' evaluation

Available Data	Indicates	Useful for
Martensite volume fraction	Austenite stability and phase transformation intensity	TRIP effect resistance
Stress-Strain curve	Yield strength, Ductility, Strain-hardening behavior	Mechanical Performance
Work-hardening rate $\left(\frac{d\sigma}{d\varepsilon}\right)$	Rate of material strengthening	TRIP-TWIP effect behavior, Ductility

4.7.1 Martensite volume fraction evolution

The diagrams depicting the evolution of α′-Martensite volume fraction under mechanical strain illustrate the distinct transformation behavior of each austenitic alloy. Among them, the Duplex stainless steel exhibits the lowest overall martensite formation. This outcome is anticipated, as the duplex alloy contains the smallest initial volume fraction of austenite, limited to 65%. Consequently, the α′-Martensite fraction cannot exceed this value, regardless of the applied strain. Among the fully austenitic grades evaluated, AISI 304L stainless steel demonstrated the most favorable response. Due to its low carbon content and balanced composition, it consistently exhibited excellent performance across all simulated temperatures, including down to −100 °C. The alloy maintained low levels of martensitic transformation preserving ductility making it a suitable candidate for low temperature structural applications. Unexpectedly the least suitable candidate is a low carbon 316L. Surprisingly, the least suitable candidate among the fully austenitic steels was found to be AISI 316L, despite its low carbon content and widespread use in cryogenic applications. While it is often selected for its enhanced corrosion

Institutional Repository - Library & Information Centre - University of Thessaly
13/09/2026 18:03:45 EEST - 216.73.216.14

resistance and phase stability due to molybdenum additions, the simulation results indicate a relatively high volume fraction of α′-Martensite formed under applied mechanical strain.

The computational MATLAB model was not capable of producing results for 316L beyond -60ºC and for AISI 201 and 316 beyond -80ºC.

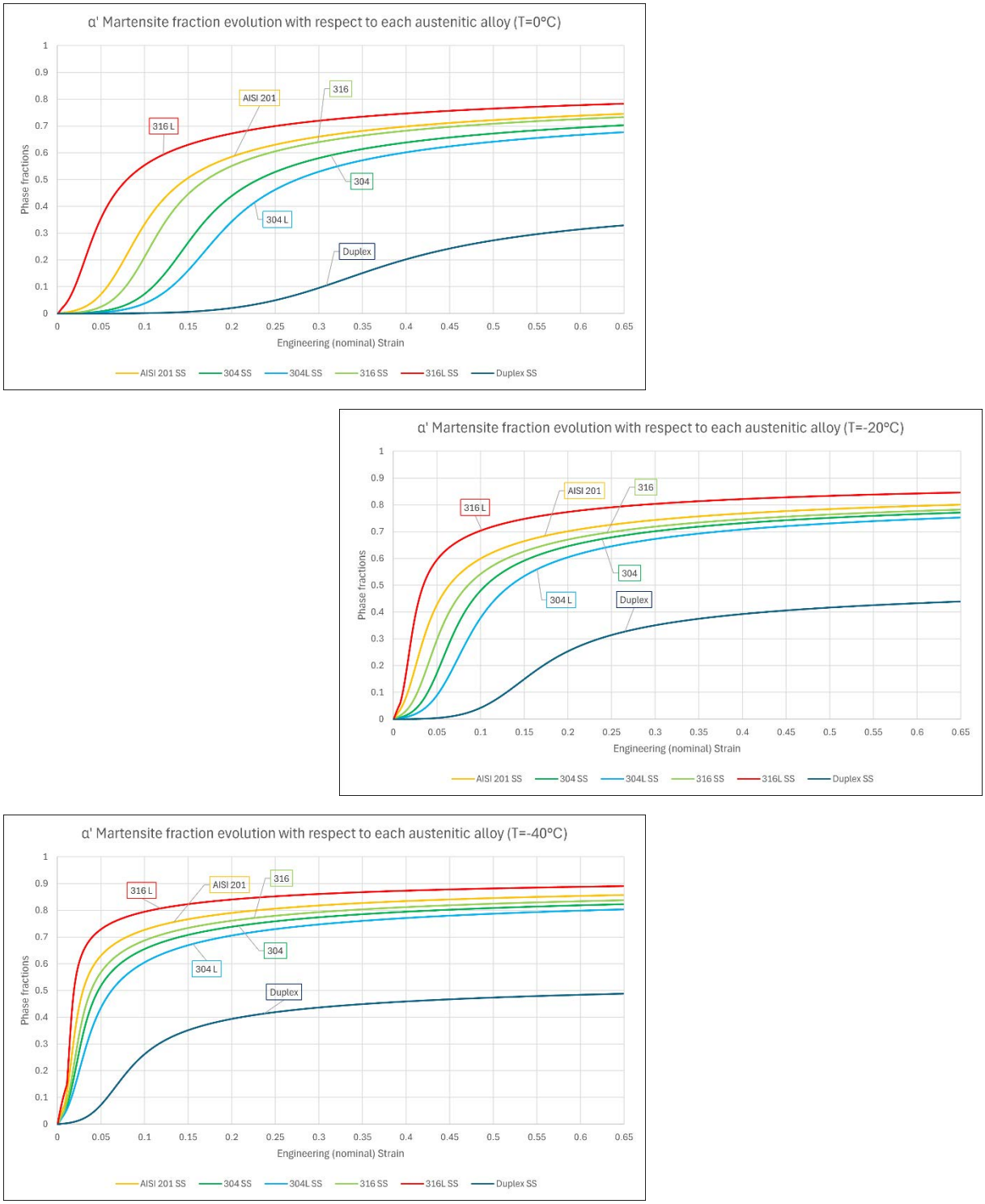

Fig. 18: Martensite fractions with respect to each examined steel at 0, -20 and -40ºC

Institutional Repository - Library & Information Centre - University of Thessaly
13/09/2026 18:03:45 EEST - 216.73.216.14

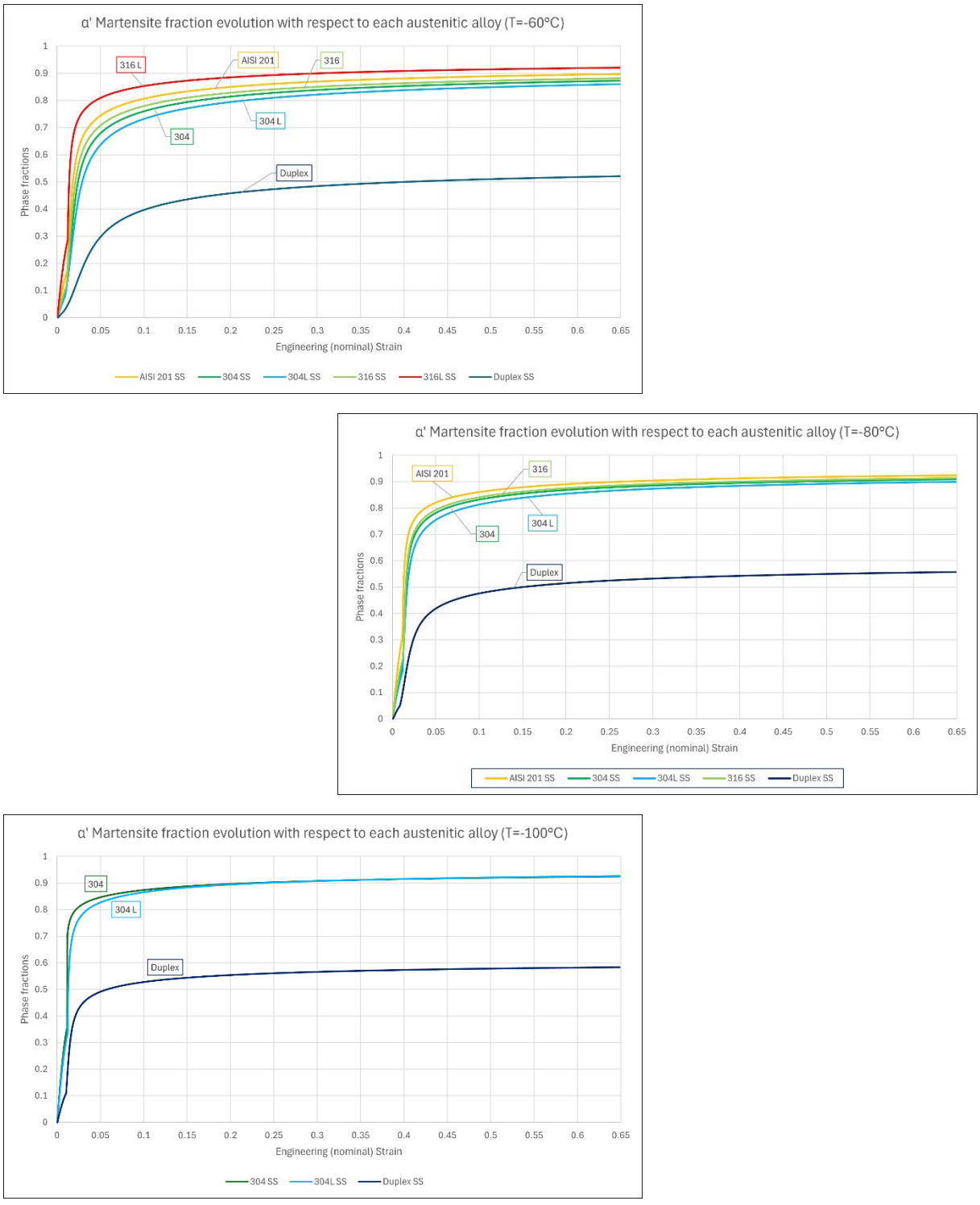

Fig. 19: Martensite fractions with respect to each examined steel at -60, -80 and -100°C

Institutional Repository - Library & Information Centre - University of Thessaly
13/09/2026 18:03:45 EEST - 216.73.216.14

4.7.2 Stress-Strain curves

The comparison continues with the analysis of the nominal and true stress–strain responses of each investigated alloy at 20 °C, as illustrated in Fig. 20. Among all alloys, AISI 316 stainless steel exhibits the highest ultimate tensile strength in both nominal and true stress plots, with a steep hardening slope and quite delayed necking, indicative of an aggressive TRIP effect. This is consistent with its high α′-Martensite fraction, but also suggests a potential compromise in ductility at lower temperatures. On the other hand, AISI 304L demonstrates a more gradual stress increase and a longer uniform elongation range, confirming its balanced mechanical performance and retained ductility.

In contrast, the duplex stainless steel, while exhibiting the lowest stress rise among the group, maintains a consistent strain response with minimal transformation, attributed to its high stacking fault energy and dual-phase stability. The true stress–strain curves further highlight these distinctions, with 316 SS achieving the highest flow stress values due to progressive martensite formation, while 316L and the duplex alloy show very early saturation, signaling limited strain hardening. These comparisons reinforce the conclusion that 304L offers the most favorable compromise between strength and deformation stability, especially in conditions where excessive transformation could undermine mechanical integrity.

So far, there appears to be a consistent correlation between the austenite transformation fraction and the mechanical response of the investigated alloys. Specifically, the plotted curves for both α′-Martensite volume fraction and stress–strain behavior follow a remarkably similar trend. The sequence in which the curves are ordered—beginning with the Duplex SS, followed by AISI 304L, 304, 316, 201, and concluding with 316L—remains consistent across both types of plots. Alloys that exhibit lower levels of martensitic transformation tend to show smoother strain hardening profiles, enhanced ductility, and more gradual stress evolution. Conversely, alloys with a high martensite fraction experience rapid strength increases followed by early saturation or strain localization.

This direct correlation suggests that the extent of phase transformation during deformation plays a critical role in shaping the alloy’s mechanical response. Alloys that resist transformation retain a more stable austenitic matrix, resulting in more favorable elastoplastic behavior-especially important for cryogenic applications where ductility and phase stability are key.

Institutional Repository - Library & Information Centre - University of Thessaly
13/09/2026 18:03:45 EEST - 216.73.216.14

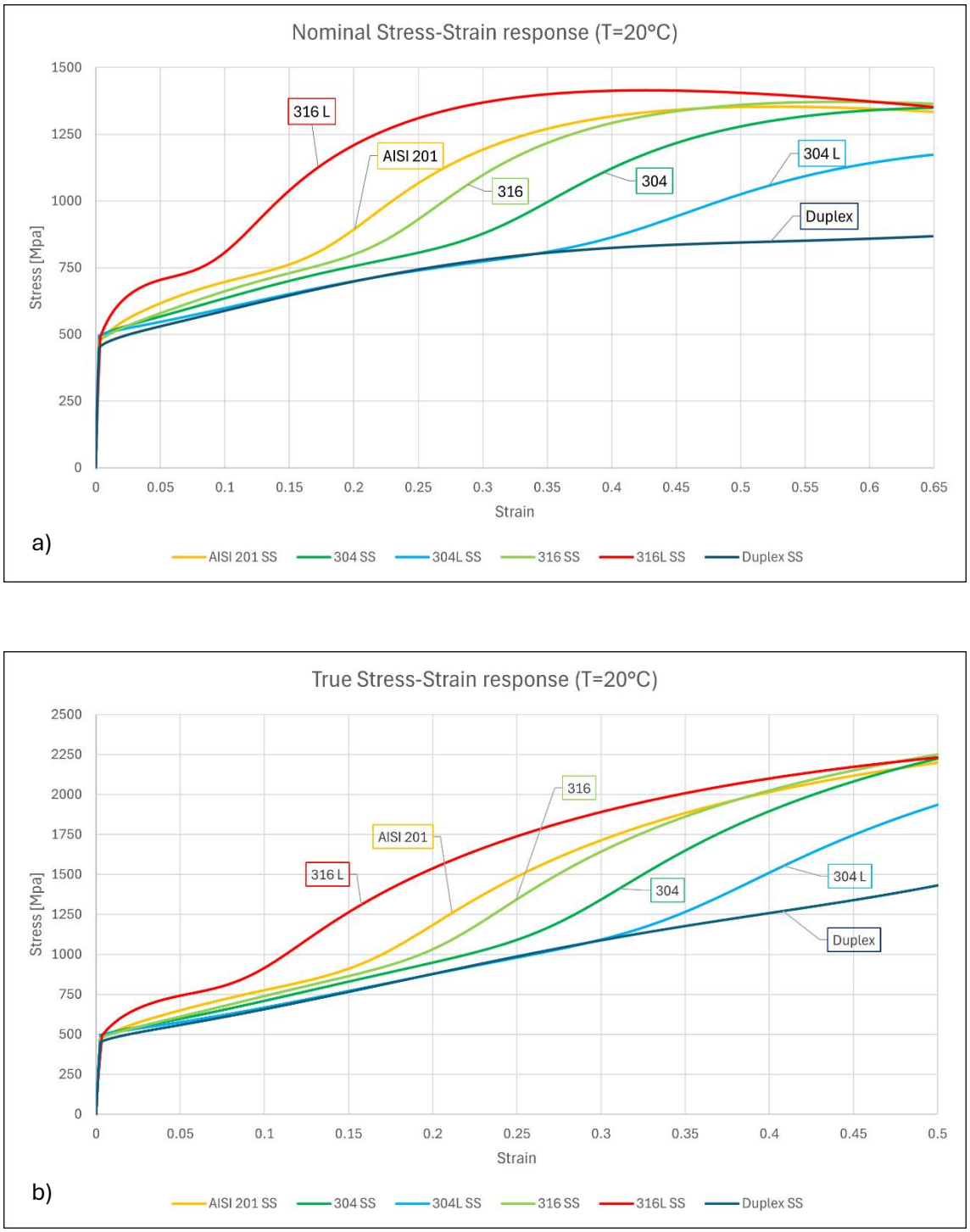

Fig. 20: Stress-Strain curves of each examined stainless steel alloy, nominal (a) and true (b)

Institutional Repository - Library & Information Centre - University of Thessaly
13/09/2026 18:03:45 EEST - 216.73.216.14

4.7.3 Work-hardening rate

Finally, the work-hardening rate $\left(\frac{d\sigma}{d\varepsilon}\right)$ of each alloy was calculated and is presented in the graph below. This parameter offers additional insight into the strain-hardening mechanisms active during deformation and further highlights the differences in transformation kinetics and mechanical stability among the studied alloys.

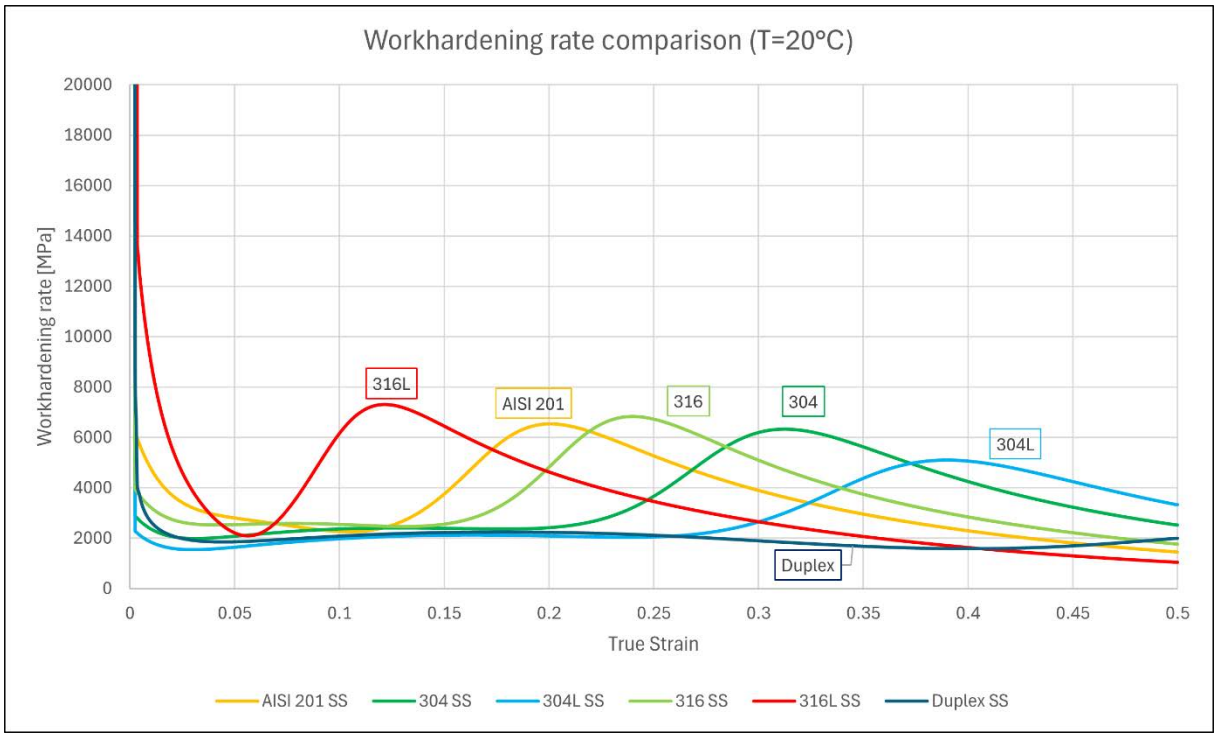

Fig. 21: Work-hardening rate of each steel examined at 20°C

The work-hardening rate curves provide a more detailed view of each alloy's deformation behavior, especially regarding the onset and evolution of transformation-induced hardening mechanisms. AISI 316 stainless steel exhibits the highest initial work-hardening rate, with a distinct peak at low strain, corresponding to a sharp increase in α′-Martensite formation. This is characteristic of a strong TRIP effect, where phase transformation contributes significantly to the material's strength. AISI 201 follows a similar trend but with a slightly delayed peak, suggesting transformation occurs at a higher strain level.

In contrast, AISI 304L and Duplex SS display smoother, more gradual hardening behavior with no abrupt peaks. This indicates a dominance of dislocation glide and twinning over martensitic transformation, consistent with their lower martensite fractions and higher austenite stability. Notably, 316L, despite its low carbon content, shows a surprisingly pronounced work-hardening peak, aligning with its unexpectedly high transformation tendency observed earlier.

The trend continues, showing the direct correlation between the transformation kinetics and work-hardening rate. The more stable austenitic phases seem to have a steady, extended hardening, retaining ductility and avoiding localization early under applied strain.

Institutional Repository - Library & Information Centre - University of Thessaly
13/09/2026 18:03:45 EEST - 216.73.216.14

Chapter 5. Conclusions and Recommendations

5.1 Conclusions

The study concluded that among the five fully austenitic stainless steel alloys investigated, AISI 304L demonstrated the most favorable behavior under mechanical strain. It exhibited the lowest final α′-Martensite volume fraction, the slowest transformation kinetics, and retained ductility, making it the most promising candidate for cryogenic applications where phase stability is essential. The available data consistently converges toward AISI 304L as the most suitable candidate among the fully austenitic stainless steels investigated.

This conclusion is supported by its low final α′-Martensite volume fraction, a balanced stress–strain response with extended uniform deformation, and a work-hardening rate curve that exhibits a characteristic hump at a relatively high strain level. This delayed onset of transformation-induced hardening reflects slow transformation kinetics, suggesting that 304L maintains a stable austenitic phase over a broader deformation range. In cryogenic or strain-intensive conditions, ductility retention is essential to ensure the structural integrity of the critical components.

However, when the custom-designed Duplex stainless steel-compositionally and structurally similar to the commercial Duplex 2205 (UNS S32205)-is included in the comparison, it emerges as the optimal alloy overall. Having a dual-phase structure, inherently high stacking fault energy, and limited austenite content (65%), the Duplex SS restricted martensitic transformation even further. This, coupled with its proven industrial application in LNG storage tanks, positions it as the most robust and transformation-resistant material among those evaluated for low-temperature mechanical performance.

5.2 Limitations of the Study

This study was conducted under certain limitations that must be acknowledged. The constitutive model implemented in MATLAB was originally designed to incorporate experimental stress–strain data and allow for parameter fitting based on user input. However, within the scope of this research, no experimental stress–strain data were available for the specific alloys under investigation. As a result, the model was used in a purely predictive mode, without parameter calibration or empirical validation. This absence of fitting may have introduced deviations between the simulated results and the actual mechanical behavior of the alloys, particularly in terms of transformation kinetics and phase fraction evolution. While the trends observed are consistent with known metallurgical principles and alloy behavior, the quantitative accuracy of the simulations should be interpreted with caution until experimental validation can be conducted.

In addition to the absence of experimental stress–strain data, several critical material parameters required by the constitutive model were not available in the literature for the specific alloys examined. These include:

- Initial nucleation site density for stress-assisted transformation (N_0^{SA})
- Dislocation generation factors for both γ-austenite and α′-Martensite (k_1^{γ}, $k_1^{\alpha'}$)

Institutional Repository - Library & Information Centre - University of Thessaly
13/09/2026 18:03:45 EEST - 216.73.216.14

- Dynamic recovery coefficients ($f_{DRV_0}^{\gamma}$, $f_{DRV}^{\alpha'}$)
- Hall–Petch strengthening coefficient of austenite (k_{γ}^{HP})
- Initial dislocation densities (ρ_{γ}^{0}, $\rho_{\alpha'}^{0}$)

Due to the lack of alloy-specific values for these parameters, the model employed default values as originally defined by John S. Aristeidakis in his doctoral thesis, which forms the basis of the current computational framework. While these default parameters were not specifically fitted for the alloys examined in this study, they have been previously validated and are known to produce physically consistent results. Their use enabled a comprehensive comparative analysis of transformation behavior and mechanical response across all investigated materials. The outcome remains valuable for comparative analysis, but absolute accuracy may be limited without experimental calibration or further parameter refinement.

5.3 Recommendations for Future Work

To further enhance the reliability and applicability of the findings presented in this study, several recommendations are proposed:

1. **Experimental Validation**: Conduct mechanical testing (e.g., tensile tests at cryogenic temperatures) on the investigated alloys to validate the predicted stress–strain responses and transformation kinetics. This would reinforce the credibility of the model results and allow for further refinement
2. **Parameter Optimization**: Determine material-specific values for critical microstructural parameters such as nucleation site density, dislocation generation and recovery rates, and initial dislocation densities through experimental methods or literature-based calibration. Replacing default values with alloy-specific data would enhance model precision
3. **Extended Alloy Screening**: Investigate additional austenitic-ferritic (duplex) grades and high-Mn steels to broaden the candidate range, particularly for hydrogen and LNG storage where performance demands are currently increasing
4. **Incorporate Multi-Physics Effects**: Include effects such as thermal cycling, residual stresses, or strain rate sensitivity in future modeling to more closely represent real service conditions
5. **Industrial Application Assessment**: Evaluate the simulated alloy behavior in the context of full-scale components (e.g., pressure vessels, cryo-piping), possibly through finite element integration of the constitutive model for structural simulation

Institutional Repository - Library & Information Centre - University of Thessaly
13/09/2026 18:03:45 EEST - 216.73.216.14

References

[1]: Aristeidakis, J. S., & Haidemenopoulos, G. N. (2020). Composition and processing design of medium-Mn steels based on CALPHAD, SFE modeling, and genetic optimization. *Acta Materialia, 193*, 291–310. https://doi.org/10.1016/j.actamat.2020.03.052

[2]: Aristeidakis, J. S., & Haidemenopoulos, G. N. (2022). Constitutive and transformation kinetics modeling of ε-, α′-Martensite and mechanical twinning in steels containing austenite. *Acta Materialia, 228*, 117757. https://doi.org/10.1016/j.actamat.2022.117757

[3]: Olson, G.B., Cohen, M. A general mechanism of martensitic nucleation: Part I. General concepts and the FCC → HCP transformation. *Metall Trans A* **7**, 1897–1904 (1976). https://doi.org/10.1007/BF02659822

[4]: Zecevic, M., Upadhyay, M. V., Polatidis, E., Panzner, T., Van Swygenhoven, H., & Knezevic, M. (2019). A crystallographic extension to the Olson–Cohen model for predicting strain path dependence of martensitic transformation. *Acta Materialia, 166*, 386–401. https://doi.org/10.1016/j.actamat.2018.12.060

[5]: Lee, S., Estrin, Y. & De Cooman, B.C. Constitutive Modeling of the Mechanical Properties of V-added Medium Manganese TRIP Steel. *Metall Mater Trans A* **44**, 3136–3146 (2013). https://doi.org/10.1007/s11661-013-1648-4

[6]: Estrin, Y., & Mecking, H. (1984). A unified phenomenological description of work hardening and creep based on one-parameter models. *Acta Metallurgica, 32*(1), 57–70. https://doi.org/10.1016/0001-6160(84)90202-5

[7]: Kocks, U. F., & Mecking, H. (2003). Physics and phenomenology of strain hardening: The FCC case. *Progress in Materials Science, 48*(3), 171–273. https://doi.org/10.1016/S0079-6425(02)00003-8

[8]: Bouaziz, O., & Guelton, N. (2001). Modelling of TWIP effect on work-hardening. *Materials Science and Engineering: A, 319–321*, 246–249. https://doi.org/10.1016/S0921-5093(00)02019-0

[9]: Galindo-Nava, E. I., & Rivera-Díaz-del-Castillo, P. E. J. (2017). Understanding martensite and twin formation in austenitic steels: A model describing TRIP and TWIP effects. *Acta Materialia, 128*, 120–134. https://doi.org/10.1016/j.actamat.2017.02.004

[10]: Papadioti, I., Bellas, I., Tzini, M.-I. T., Christodoulou, P. I., & Aravas, N. (2020). TRIP Steels: A Multiscale Computational Simulation and Experimental Study of Heat Treatment and Mechanical Behavior. *Materials*, *13*(2), 458. https://doi.org/10.3390/ma13020458

[11]: Tzini, M.-I. T., Aristeidakis, J. S., Christodoulou, P. I., Kermanidis, A. T., Haidemenopoulos, G. N., & Krizan, D. (2022). Multi-phase field modeling in TRIP steels: Distributed vs. average stability and strain-induced transformation of retained austenite. *Materials Science and Engineering: A, 833*, 142341. https://doi.org/10.1016/j.msea.2021.142341

[12]: Haidemenopoulos, G. N., Aravas, N., & Bellas, I. (2014). Kinetics of strain-induced transformation of dispersed austenite in low-alloy TRIP steels. *Materials Science and Engineering: A, 615*, 416–423. https://doi.org/10.1016/j.msea.2014.07.099

Institutional Repository - Library & Information Centre - University of Thessaly
13/09/2026 18:03:45 EEST - 216.73.216.14

[13]: Pierce, D. T., Jiménez, J. A., Bentley, J., Raabe, D., Oskay, C., & Wittig, J. E. (2014). The influence of manganese content on the stacking fault and austenite/ε-martensite interfacial energies in Fe–Mn–(Al–Si) steels investigated by experiment and theory. *Acta Materialia, 68*, 238–253. https://doi.org/10.1016/j.actamat.2014.01.001

[14]: Allain, S., Chateau, J.-P., Bouaziz, O., Migot, S., & Guelton, N. (2004). Correlations between the calculated stacking fault energy and the plasticity mechanisms in Fe–Mn–C alloys. *Materials Science and Engineering: A, 387–389*, 158–162. https://doi.org/10.1016/j.msea.2004.01.059

[15]: Hillert, M., & Jarl, M. (1978). A model for alloying in ferromagnetic metals. *Calphad, 2*(3), 227–238. https://doi.org/10.1016/0364-5916(78)90011-1

Appendix. Supplementary Materials

Download: Transformation_Kinetics_Model.zip

Download: SFE_Model.zip

Institutional Repository - Library & Information Centre - University of Thessaly
13/09/2026 18:03:45 EEST - 216.73.216.14